Posted on 30 Nov 2022 — The copyright holder is the author/funder. All rights reserved. No reuse without permission. — https://doi.org/10.1002/essoar.10501592/v2 — This a preprint and has not been peer reviewed. Data may be preliminary.

The Polar Cap (PC) index: invalid index series and a different approach.

Peter Stauning[1,1]

[1]Danish Meteorological Institute

November 30, 2022

Abstract

The Polar Cap (PC) indices are derived from the magnetic variations generated by the transpolar convection of magnetospheric plasma and embedded magnetic fields driven by the interaction with the solar wind. The PC indices are potentially very useful for Space Weather monitoring and forecasts and for related research. However, the PC index series in the near-real time and final versions endorsed by the International Association for Geomagnetism and Aeronomy (IAGA) are considered unreliable. Both versions include solar wind sector (SWS) effects in the calculation of the reference levels from which magnetic disturbances are measured. The SWS effects are caused by current systems in the dayside Cusp region related to the Y-component, B, of the Interplanetary Magnetic Field (IMF). However, the IAGA-endorsed handling of SWS effects may generate unfounded PC index changes of up to 3 mV/m at the nightside away from the Cusp. For the real-time PCN and PCS indices, the cubic spline-based reference level construction may cause additional unjustified index excursions of more than 3 mV/m with respect to the corresponding final index values. Noting that PC index values above 2 mV/m indicate geomagnetic storm conditions, such unjustified contributions are considered to invalidate the IAGA-endorsed PC index series. Alternative derivation methods are shown to provide more consistent index reference levels for both final and real-time PC indices, to reduce their unfounded excursions, and to significantly increase their reliability.

Revised manuscript 27 January 2020/PSt

The Polar Cap (PC) index: invalid index series and a different approach.

Peter Stauning
Danish Meteorological Institute, Copenhagen, Denmark
Mail: pst@dmi.dk

Abstract.

The Polar Cap (PC) indices are derived from the magnetic variations generated by the transpolar convection of magnetospheric plasma and embedded magnetic fields driven by the interaction with the solar wind. The PC indices are potentially very useful for Space Weather monitoring and forecasts and for related research. However, the PC index series in the near-real time and final versions endorsed by the International Association for Geomagnetism and Aeronomy (IAGA) are considered unreliable. Both versions include solar wind sector (SWS) effects in the calculation of the reference levels from which magnetic disturbances are measured. The SWS effects are caused by current systems in the dayside Cusp region related to the Y-component, B_Y, of the Interplanetary Magnetic Field (IMF). However, the IAGA-endorsed handling of SWS effects may generate unfounded PC index changes of up to 3-4 mV/m at the nightside away from the Cusp. For the real-time PCN and PCS indices, the cubic spline-based reference level construction may cause additional unjustified index excursions of more than 3 mV/m with respect to the corresponding final index values. Noting that PC index values above 2 mV/m indicate geomagnetic storm conditions, such unjustified contributions are considered to invalidate the IAGA-endorsed PC index series. Alternative derivation methods are shown to provide more consistent index reference levels for both final and real-time PC indices, to reduce their unfounded excursions, and to significantly increase their reliability.

1. Introduction.

The Polar Cap (PC) indices, PCN (North) and PCS (South) are based on magnetic data recorded at the central polar cap observatories in Qaanaaq (Thule) in Greenland and Vostok in Antarctica, respectively. The PC index concept was developed through the pioneering works of Troshichev and Andrezen (1985) and Troshichev et al. (1988). Further PC index developments were made by Vennerstrøm (1991). A fundamental description of the PC index derivation methods and their physical meaning was published by Troshichev et al. (2006).

To derive PC index values, magnetic variations related to the transpolar convection of plasma and magnetic fields are calibrated to equal values of the merging electric field (Kan and Lee, 1979) in the undisturbed solar wind. Thus, the PC indices represent the merging processes between the solar wind magnetic fields extending from the Sun and the terrestrial magnetic fields at the front of the magnetosphere and could be considered representative of the energy input from the solar wind. This energy may be temporarily stored in the magnetospheric tail configuration to be dissipated in processes such as auroral substorms, upper atmosphere heating, and ring current enhancements.

Final (post-event) PCN and PCS index series have been used to investigate relations between interplanetary parameters and polar cap magnetic disturbances (e.g., Troshichev and Lukianova, 2002; Huang, 2005) and the electric potentials in the polar cap ionosphere (e.g., Troshichev et al., 2000; Nagatsuma, 2002; Ridley and Kihn, 2004).

The relations between the polar cap indices and auroral activity was studied, among others, by Troshichev and Andrezen (1985), Vennerstrøm et al. (1991), Vassiliadis et al. (1996), Liou et al. (2003), and Huang (2005). The relations between positive and negative PC index values and Joule heating of the atmosphere was investigated by Chun et al. (1999, 2002). Most investigations have given correlation coefficients ranging between 0.6 and 0.8 between polar cap index values and parameters characterizing auroral activity.

In substorm studies, Janzhura et al. (2007) have used the PC indices to predict the duration of the growth phase in substorm developments. For isolated events they estimated that substorm onset would occur as the PC index level reached ~2 mV/m From investigations of a large number of substorms, Troshichev et al. (2014) concluded that substorm onset was likely to happen when the PC index starting from a low level exceeded 1.5 ±0.5 mV/m.

In studies of geomagnetic storms by Stauning et al. (2008) and Stauning (2012), the PC indices have been used in source functions to predict the development of ring current intensities characterized by Dst index values. Troshichev and Sormakov (2017) have used PC indices to predict the maximum geomagnetic storm intensities (Dst minima).

An important application of real-time PC indices is the forecast of strong substorms that may threaten power grids through their Geomagnetically Induced Current (GIC) effects. An investigation of GIC-related high voltage power line disturbances in Scandinavia (Stauning, 2013c) has demonstrated that the PC index values most often remained at a high level for more than 2-3 hours up to the power line cuts. The lengthy pre-event intervals are most likely needed for enabling the merging processes at the front of the magnetosphere and subsequent transpolar convection characterized by the PC index to load the tail configuration with enough energy to generate violent substorm events. The intense merging processes may also be necessary for making the polar cap expand enough to enable substorm activity reaching subauroral latitudes where important power grids reside. According to these investigations, PC index levels above 10 mV/m maintained through more than one hour should cause alert for subauroral power grids (Stauning, 2020).

In the past, a diversity of PC index versions have been in play at the above-mentioned (and many further) investigations (Stauning, 2013a), which seriously reduce their scientific value. Thus, much

effort has been invested in attempts to generate commonly accepted PC index versions (e.g., Troshichev et al., 2006; Stauning et al., 2006). On basis of the documentation provided in Matzka (2014), new PC index versions were adopted by IAGA by its Resolution no. 3 (2013) with the text:

*IAGA, **noting** that polar cap magnetic activity is not yet described by existing IAGA geomagnetic indices, **considering** that the Polar Cap (PC) index constitutes a quantitative estimate of geomagnetic activity at polar latitudes and serves as a proxy for energy that enters into the magnetosphere during solar wind-magnetosphere coupling, **emphasising** that the usefulness of such an index is dependent on having a continuous data series, **recognising** that the PC index is derived in partnership between the Arctic and Antarctic Research Institute (AARI, Russian Federation) and the National Space Institute, Technical University of Denmark (DTU, Denmark) **recommends** use of the PC index by the international scientific community in its near-real time and definitive forms, and **urges** that all possible efforts be made to maintain continuous operation of all geomagnetic observatories contributing to the PC index.*

Thus, the IAGA-recommendations comprise both the final and the near-real time versions of PCN and PCS indices. Until the final values could be issued, the indices may be available in provisional versions. At present, the PCN indices are distributed in all versions, while the PCS indices are distributed in their near-real time and provisional versions only. The indices are distributed from the web portals http://pcindex.org operated by AARI and http://isgi.unistra.fr operated by the International Service for Geomagnetic Indices (ISGI). However, as shall be demonstrated, the near-real time values as well as the final PC index series are invalidated by inappropriate handling of the solar wind sector effects in reference level calculations.

2. Calculation of Polar Cap indices.

The transpolar (noon to midnight) convection of plasma and magnetic fields driven by the interaction of the solar wind with the magnetosphere generates electric (Hall) currents in the upper atmosphere. These currents, in turn, induce magnetic variations at ground level (Troshichev et al., 1988, 2006; Vennerstrøm, 1991). For derivation of PC indices from the recorded magnetic field series, $\mathbf{F}$, the horizontal magnetic variations, $\Delta\mathbf{F} = \mathbf{F} - \mathbf{F}_{RL}$, with respect to an undisturbed reference level (RL), $\mathbf{F}_{RL}$, are projected to a direction in space assumed to be perpendicular to the transpolar convection-related currents in order to focus on solar wind effects. The optimum direction is characterized by its angle, φ, to the E-W direction. Next, ΔF_{PROJ} values are scaled to make the PC index equal on the average to the solar wind merging electric field, E_M, (Kan and Lee, 1979). Thus

$$PC = (\Delta F_{PROJ} - \beta)/\alpha \approx E_M \quad (1)$$

The optimum angle, φ, and the propagation delay, τ, between the reference location for the solar wind data and the location for related effects at the polar cap are both estimated from searching the optimum correlation between E_M and $\Delta F_{PROJ.}$ The calibration constants, the slope, α, and the intercept, β, are found by linear regression between ΔF_{PROJ} and E_M through an extended epoch of past data.

3. PC index reference level.

For the reference level from which polar magnetic disturbances are measured, different concepts have been used. In the version developed by Vennerstrøm (1991), just the secularly varying base level, $\mathbf{F}_{BL}$, was used. This level does not reflect the daily magnetic variations during undisturbed conditions. However, the calibration parameters, notably the intercept coefficient, reflect the undisturbed daily variation averaged over the epoch used for the regression.

120 $\mathbf{F}_{RL} = \mathbf{F}_{BL}$ (Vennerstrøm, 1991) (2)

121 In the version developed at the Arctic and Antarctic Research Institute (AARI) in St. Petersburg,
122 Russia, the varying level on "*extremely quiescent days*" (Troshichev et al., 2006) was used as the
123 PC index reference level. This level could be considered built from a quiet day curve (QDC), $\mathbf{F}_{QDC}$,
124 added on top of the base level, $\mathbf{F}_{BL}$. Thus in vector formulation:

125 $\mathbf{F}_{RL} = \mathbf{F}_{BL} + \mathbf{F}_{QDC}$ (AARI, Troshichev et al., 2006) (3)

126 Extremely quiescent days are rare particularly at polar latitudes. Therefore, the concept was
127 broadened to imply the generation of QDC values from quiet segments of nearby days. The QDC
128 calculations are detailed in Janzhura and Troshichev (2008) (hereinafter J&T2008). From the
129 recordings during 30 days at a time, the variability in the 1-min samples within each 20-min section
130 of recorded data is used to decide whether the section is quiet enough to let the average value be
131 included in the construction of an initial QDC by superposition of quiet samples. The particular day
132 for the QDC is determined by the relative amounts of quiet samples and usually positioned at the
133 middle of the considered interval. The 30 days interval is then shifted forward and the QDC
134 calculations repeated to be referred to another (or eventually the same) day. Finally, from the
135 sequence of initial 30-days QDCs the final QDCs for any of the days are found by smoothing
136 interpolation. It should be noted that the choice of using 30 days interval at a time implies evening
137 out possible solar wind sector (SWS)-related effects which may have cyclic variations with the 27.4
138 days solar rotation. (the notation "SWS" is used here instead of "SS" used elsewhere).

139 In order to handle the SWS-related variations, $\mathbf{F}_{SWS}$, caused mainly by the effects from the Y-
140 component, IMF B_Y, of the Interplanetary Magnetic field (IMF), on the convection patterns, it was
141 suggested by Menvielle et al. (2011) that the reference level should be constructed from using a
142 particular solar wind sector term, $\mathbf{F}_{SWS}$, added to the base level and the regular QDC.

143 $\mathbf{F}_{RL} = \mathbf{F}_{BL} + \mathbf{F}_{QDC} + \mathbf{F}_{SWS}$ (Menvielle et al., 2011) (4)

144 It should be noted that this concept marks an infringement of the QDC definition in Troshichev et
145 al. (2006) by introducing a reference level contribution, $\mathbf{F}_{SWS}$, which is not necessarily quiet. There
146 is no validation of this concept or reference to its origin in Menvielle et al. (2011).

147 The SWS concept is further specified in Janzhura and Troshichev (2011) (hereinafter J&T2011). At
148 the interaction between the solar wind and the magnetosphere, as explained in J&T2011, the IMF
149 B_Y components generate field-aligned currents (FAC) and associated horizontal currents in the
150 Cusp region near local noon at 75-80° geomagnetic latitude. In p. 1492 of J&T2011 they state that
151 "*the QDC level displays long-term changes, which are determined by the sector structure*". Further
152 they state "*Thus, if we are going to analyze the polar cap magnetic activity produced by the IMF*
153 *fluctuations related to disturbed solar wind, we have to exclude first the sector structure effect*".

154 One implication of their statement is that the IMF B_Y component when varying slowly (few days to
155 2 weeks) is not affecting the polar magnetic disturbance levels. The issue has not been properly
156 validated and the implication might be incorrect. The second issue, which shall be discussed to
157 some extent here, is whether the applied data handling techniques actually remove the sector
158 structure effects or just (as will be shown) generate inconsistent features and odd results.

159 In J&T2011 the sector structure effects are derived from daily median values of the recorded polar
160 magnetic fields that vary with the IMF B_Y component in the solar wind. In the post-event version,
161 the SWS terms are derived from daily median values smoothed over 7 days with the day of interest
162 at the middle. In the near-real time version the actual day's SWS value is derived by cubic spline-
163 based extrapolation of past daily median values. The regular 30-days QDC is derived from the
164 recorded data less the SWS effect. Thus:

$$\mathbf{F}_{RL} = \mathbf{F}_{BL} + \mathbf{F}_{SWS} + \mathbf{F}_{QDC,SWS} \quad \text{(Janzhura and Troshichev, 2011)} \quad (5)$$

For the IAGA-endorsed version (Matzka, 2014), the base level in the AARI version in Eq. 3 (Troshichev et al., 2006) is replaced by a median-based level, $\mathbf{F}_M$. The modified QDC term, $\mathbf{F}_{QDC,SWS}$, is derived from the data series, $\mathbf{F}$, less the $\mathbf{F}_M$ values.

$$\mathbf{F}_{RL} = \mathbf{F}_M + \mathbf{F}_{QDC,SWS} = \mathbf{F}_{BL} + \mathbf{F}_{SWS} + \mathbf{F}_{QDC,SWS} \quad \text{(IAGA, Matzka, 2014)} \quad (6)$$

Actually, this is the same concept as the one defined in J&T2011 except that the secular variations are now included in the median values (Nielsen and Willer, 2019) instead of being included in the base line values. Thus, the IAGA concept could be discussed on basis of the J&T2011 publication, which – so far – holds the only existing presentation of the QDC and SWS properties issued from the providers of the IAGA endorsed PC indices. The SWS concept has been discussed in Stauning (2013b, 2015, and 2018a,c).

4. Reference levels for PC index calculations in the IAGA-endorsed post-event (final) version.

The IMF B_Y-related variations in the daily course of the polar magnetic field components are important for calculations of the reference level for PC index calculations. It should be noted that the local time 24 h cycle represents the daily course in the observatory position relative to the Cusp region located close to local noon at magnetic latitudes a few degrees equatorward of Qaanaaq latitude.

Like noted at p. 1492 in J&T2011, "*the azimuthal IMF component controls the BY FAC* (field-aligned current) *system observed in the day-time cusp region during the summer season*". Thus, the anticipated IMF B_Y-related effects on the convection patterns should maximize near noon and be reduced near midnight when the observatory location is farthest away from the Cusp. For Qaanaaq data this tendency is seen most clearly in displays of the H- (or Y-) component variations.

The interval from days 145 to 245 of 2001 is discussed in J&T2011 and therefore selected for a closer examination of data and derived values here. Fig. 5b of J&T2011 displays the average daily variations in the H-components (all samples) recorded at Qaanaaq during the summer months, May-August, of 2001 for different levels of IMF By. For the same data interval, Fig. 1 here displays the corresponding IMF B_Y-related daily variations for the quietest days only. Values of the IMF B_Y component are derived from OMNIweb interplanetary satellite data service (http://omniweb.gsfc.nasa.gov).

The results in Fig. 1 are largely the same as those of Fig. 5b in J&T2011. Local midnight at Qaanaaq is at around 04 UT, noon at 16 UT. It is seen in both diagrams that the variations with IMF B_Y are small during the night while the daytime values, and thus the amplitude in the daily variations, depend strongly on the IMF By level.

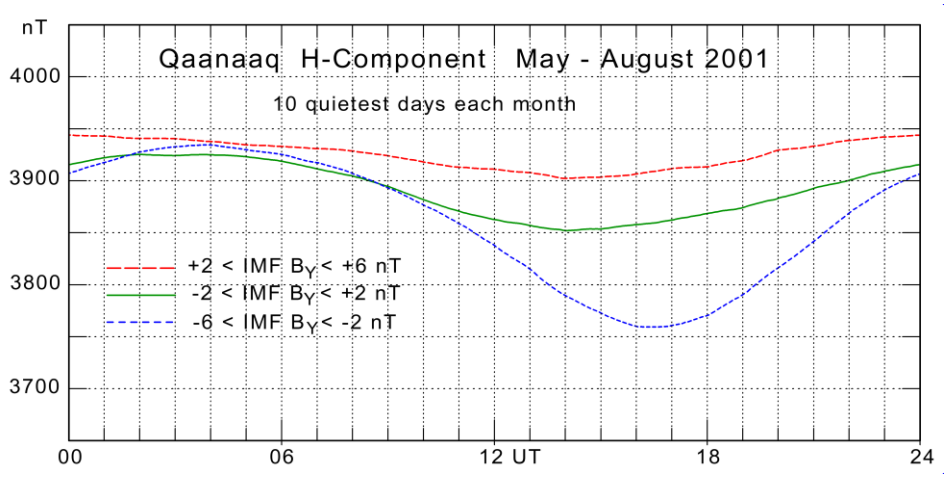

Figure 1. Mean daily variation in the H-component at Qaanaaq (Thule) during the 10 quietest days of each of the summer months of 2001 derived for three gradations of the IMF azimuthal component: +2 < B_Y <+6 nT (upper red line), -2< B_Y <2 nT (green line), and -6 < By <-2 nT (lower blue line).

With the variations of the QDC values with IMF B_Y displayed in Fig. 1 during the months centered on 1 July and corresponding displays centered at different dates, the QDC values throughout the selected interval could be constructed. The resulting QDCs taking the seasonal as well as the IMF B_Y-related variations into account are displayed by the curve in heavy red line superimposed on the observed values of the H-component shown in Fig. 2. Smoothed values of IMF B_Y are displayed by the lover curve with reference to the right scale. The upper envelope of the QDC values presents the night H-component values and varies little with IMF B_Y while the lower envelope, which presents the midday QDC values, varies strongly with IMF B_Y in agreement with the display in Fig. 1. These QDCs could be considered to represent idealized QDC levels for the summer season of year 2001.

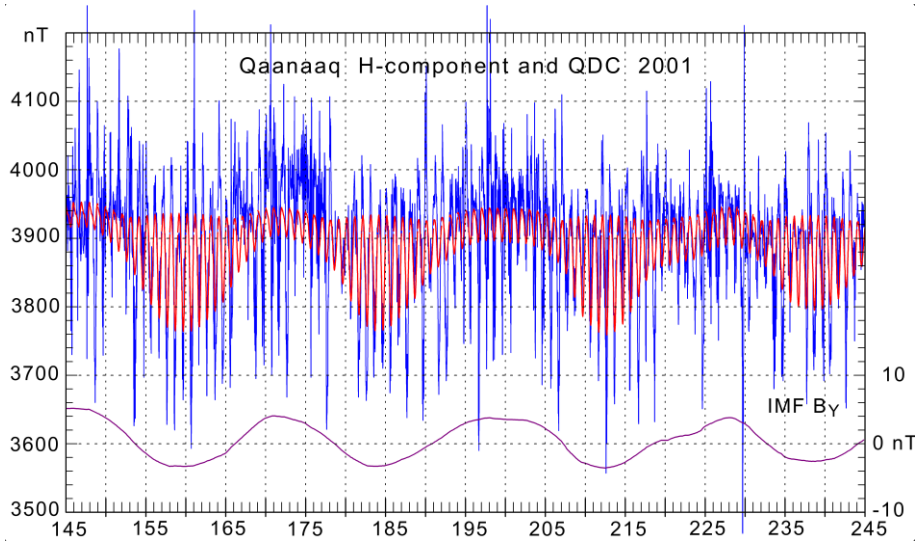

Figure 2. QDCs (red line) based on quiet data only superimposed on recorded H-component values (blue line). Smoothed values of IMF B_Y (magenta line) on right scale are shown at the bottom.

For the IAGA-endorsed post-event (final) PC index version, Fig. 3 displays the construction of the reference levels. The upper three fields are based on interim values derived from PCN index calculations and supplied from the PCN index provider at DTU Space. For reference, the bottom curve (f) displays smoothed values of the IMF B_Y component (same as those displayed in Fig. 2).

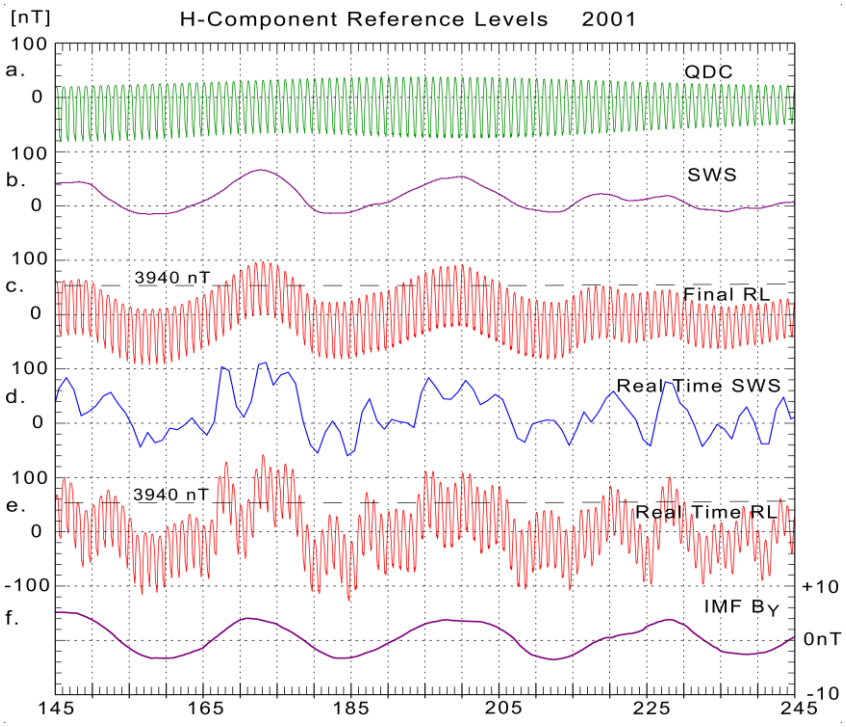

Figure 3. IAGA-endorsed constructions of H-component reference levels for PCN throughout days 145 to 245 of 2001 for final and real-time PCN index versions. (a.) Final QDC_{SWS}. (b.) Final SWS terms. (c.) Final reference levels, RL. (d.) Real-time SWS terms. (e.) Real-time reference levels. (f.) Smoothed IMF B_Y (on right scale).

The upper curve (a) in Fig. 3 displays the 30-days QDC_{SWS} values for the Qaanaaq H-component derived according to the method defined in J&T2008 but based on recorded quiet data less the SWS terms. The next lower curve (b) displays the SWS terms derived as the differences (cf. Eq. 6) between the 7-days smoothed daily median values and the secularly varying base line values interpolated between the yearly defined values (also supplied from DTU Space). The 0 nT dotted line represents base line values varying between 3895 nT on day 145 and 3899 nT on day 245.

The next lower curve (c) displays the resulting H-component reference level formed as the sum of the H_{SWS} and $H_{QDC,SWS}$ values (cf. Eq. 5). The horizontal dashed line across this curve (c) presents the uppermost level (3940 nT) of the mean H-component values in Fig. 1 (or Fig. 5 of J&T12011). Curve (c) is an almost exact replica of the H-component reference curve displayed in heavy line in Fig. 1 of J&T2011 for which the caption states "*the quiet daily curve (QDC) characterizing the daily variation of the quiet geomagnetic field*". However, there are serious problems with this choice of reference level:

(i) Contrary to the caption for Fig. 1 of J&T2011, the reference level is not "quiet" being composed from the sum of a quiet part and a median-based part that varies with the disturbance level.

(ii) The daily variations in the components imposed by the reference level construction are not in agreement with observed daily variations during corresponding conditions.

(iii) The upper envelope which represents night values of the daily variations in the H-component varies strongly with the varying IMF B_Y level contrary to night values in Fig. 1 (or Fig. 5 of J&T2011). Some of the night reference values exceed considerably the uppermost statistical average values for corresponding IMF B_Y conditions whether based on all data (Fig. 5 of J&T2011) or just quiet values (Fig. 1 here).

(iv) The amplitudes in the daily variation display seasonal variations only and do not vary with the IMF B_Y level contrary to the strong amplitude variations seen in Fig. 1 (or Fig. 5 of J&T2011). For June (days 152-181) of 2001 the amplitudes in the reference level variations remain at appr. 100 nT, while in Fig. 1 the amplitudes vary with the relevant IMF B_Y levels (-3 to +4 nT) between appr. 50 and 150 nT.

(v) Using the reference levels from Fig. 3 and the corresponding levels for the D-component at index calculations generates peculiar daily variations in the SWS-related contributions to the PCN index.

The SWS term, $\mathbf{F}_{SWS}$, is a vector rotating with the Earth and must be projected to the optimum direction in space to derive its contribution to the PC index. During 24 hours the projected term varies between + and – the maximum amplitude reached at two locations, one at daytime the other at night, when the $\mathbf{F}_{SWS}$ direction is parallel (or antiparallel) to the optimum direction. According to Eq. 1, the effect on the PC index is $\Delta PC_{SWS} = F_{SWS,PROJ} / \alpha$. The slope values, α, are around two times larger at day than at night (cf. coefficient tables at http://pcindex.org). Thus, with the present calculation scheme, the nighttime ΔPC_{SWS}, inevitably, will be around twice the daytime contributions although the IMF B_Y-related SWS effects caused by current systems at the Cusp region near noon in local time (Wilhjelm et al., 1972; Iijima and Potemra, 1976) should maximize there and be minimal at night. This obvious conflict was addressed in Stauning (2013b and 2015).

Using both the H- and the D-components (or the X- and Y-components) of the data supplied from DTU Space enables specific calculations of the SWS effects on the PCN indices. The calibration parameters (φ,α,β) published at http://pcindex.org by the index providers have been used in the calculation of the contributions. The result for a selected day, 22 June 2001, is shown in Fig. 4.

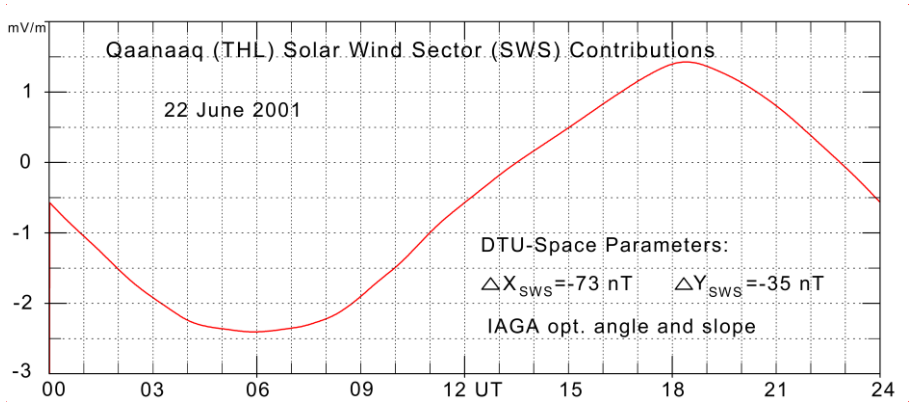

Figure 4. Variations in the SWS-related contributions to the PCN index on 22 June 2001 based on data and base line values supplied from DTU Space. (similar to Fig. 4 of Stauning, 2015)

The display in Fig. 4 based on the data supplied from DTU Space is very close to the results presented in Fig. 4 of Stauning (2015) based on the data presented in J&T2011. The most controversial feature is the (numerical) maximum in the IMF B_Y-related SWS contributions to the PCN index values at night with a depression of 2.5 mV/m at 06:30 UT near local midnight (04 UT). At this time, the THL observatory is farthest away from the Cusp region where the IMF B_Y-related effects originate. The contribution is small at local noon (16 UT) where the observatory is closest to the Cusp region. The largest positive contribution of 1.5 mV/m is seen at 18:30 UT, a few hours past local noon.

A basic error in the method is the implied assumption that a SWS term calculated from daily median values can be applied throughout the whole day to remove SWS effects disregarding the variations of the IMF B_Y–related solar wind sector effects with the varying observatory position in

the polar cap. The real SWS effects could even be opposite of the effects calculated from the constructed SWS values derived by the median-based method.

The example calculations displayed in Fig. 4 were based on the case presented in J&T2011 with a smoothed IMF B_Y value of 4 nT, which is not uncommon. Unjustified SWS contributions of 3-4 mV/m could be expected for the stronger cases (larger IMF B_Y). Such magnitudes are around twice the onset level of around 2 mV/m for magnetic storm or substorm activity (Troshichev et al., 2014).

5. Reference levels for PC index calculations in the IAGA-endorsed near-real time version.

For real-time calculations of PC index values, which is an important issue for Space Weather monitoring and forecasting, the 7-day smoothing of median values used for the final version is no longer applicable. Instead, a cubic spline extrapolation method specified in J&T2011 is applied to derive the actual SWS terms from past median values. The method uses 3-days average median values calculated every other of the past 9 days to derive cubic spline polynomials, which are subsequently extended forward to define the actual SWS value. Based on data from the examined interval of June 2001, the method is illustrated in Fig. 5 using the terminology from J&T2011.

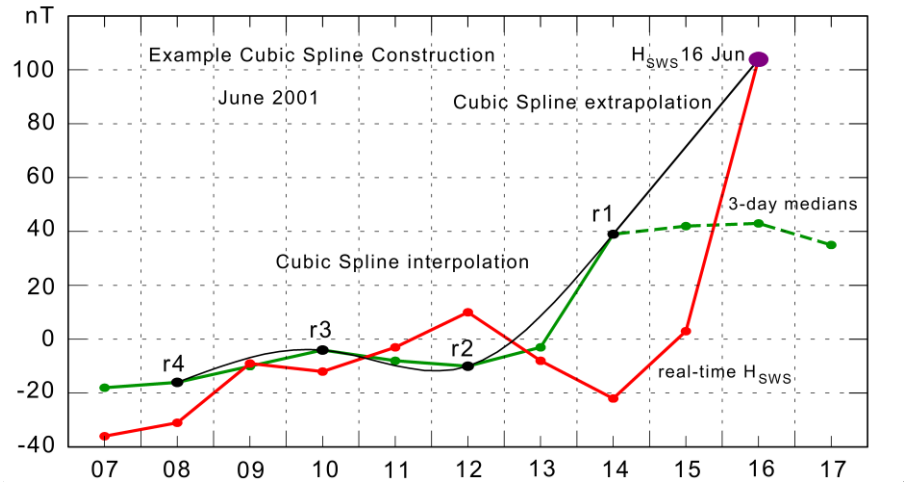

Figure 5. Details of the cubic spline construction (in black line) of the real-time solar sector term, H_{SWS}, from 3-day medians (in green line). The selected four 3-day median values used for the construction of H_{SWS} on 16 June 2001 are marked by black dots superimposed on the green ones. The cubic spline interpolation curve and its extrapolation to define real-time H_{SWS} on 16 June are displayed in black line. The dots connected by the red line represent H_{SWS} values derived by the same method on earlier dates in June 2001.

Fig. 5 demonstrates the cubic spline construction for deriving the SWS term on 16 June, 2001. The 3-day median values (green dots) named according to the J&T2011 procedure by r1 (13-15), r2 (11-13), r3 (9-11), and r4 (7-9 June) are marked by black dots superimposed on the green ones. The natural cubic spline polynomials have been derived from these 4 points and define the curve in black line connecting the points. With the slope defined at the last point (14 June) the cubic spline construction is extended tangentially to 16 June where the resulting H_{SWS} value (103 nT) is marked by a large black dot.

The dots (red) connected by a red line display the H_{SWS} values derived the same way for further days within the interval from 7 to 16 June using past data only. The 3-day median values on 15, 16 and 17 June connected by the green dashed line segments were not available at the real-time construction of H_{SWS} for 16 June. They have been added to the figure for illustration of the "take-off" effects of the cubic spline extrapolation construction that generates the large deviation of the

extrapolated SWS values compared to the post-event smoothed values (cf. Figs. 3 and 6). This is an inherent effect when using the devised "near-real time" method from J&T2011 to calculate solar sector effects. A similar figure for a different interval may be seen in Stauning, 2018c.

The real time H_{SWS} values for 7-16 June 2001 displayed in Fig. 5 along with the corresponding H_{SWS} values calculated the same way for the remainder of the days 145-245 of 2001 have been inserted as the jagged curve (d) in Fig. 3. It should be noted that these values differ from the values presented by the smooth H_{SS} curve in Fig. 6 of J&T2011, which appear, contrary to their statements in p. 1496, to be derived from smoothed median values like the nearly identical values (from DTU Space) displayed by curve (b) in Fig 3. (for the review process, please see an extended examination in appendix A1)

According to the principles for near-real time PC index calculations defined in J&T2008, the 30-days QDC should be derived by adjusting the most recent 30-days QDC using the seasonal trend from last year's QDCs. Since the QDCs in the formulation of J&T2011 (or Matzka, 2014) are derived from observed data less the SWS terms there is an obvious flaw in the arguments since the SWS-conditions are not necessarily the same at corresponding dates in different years.

Taking a short-cut by assuming that the actual near-real time $H_{QDC,SWS}$ values are the same as the final $H_{QDC,SWS}$ values displayed by curve (a) of Fig. 3 results in the near-real time H-component reference level displayed by curve (e) in Fig. 3. The corresponding process would provide the D-component near-real time values. It is clear from comparing the reference levels defined for the final version (curve c of Fig. 3) with those of the near-real time version (curve e) that PCN values calculated by the near-real time method must differ considerably from index values derived by the post-event method. The resulting effects on the differences between real-time and post-event (final) PCN values throughout June 2001 are displayed in the bottom panel of Fig. 6.

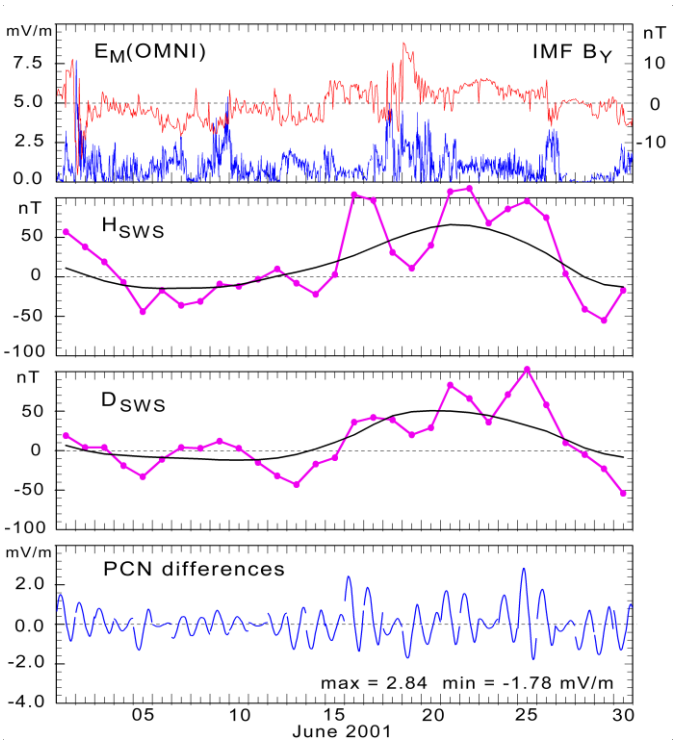

Figure 6. From top: Solar wind merging electric field (blue line, left scale) and IMF B_Y component (red line, right scale), H_{SWS} (real-time) in magenta line and H_{SWS} (final) in black line, D_{SWS} (real time) and D_{SWS} (final), and (in bottom panel) differences between real-time and final PCN values. Peak differences are noted.

The differences of up to 2.84 mV/m have been calculated from the final (smoothed) and the near-real time cubic spline extrapolated SWS vectors using consolidated calibration parameters (http://pcindex.org). The calculated examples agree well with results obtained from occasional downloads of near-real time PCN and PCS values compared to the same index series downloaded at much later times. Differences of up to 3.09 mV/m for PCN (Stauning, 2018c) and up to 3.67 mV/m for PCS (Stauning, 2018a) were found in the examples displayed in Fig. 7. Such differences related to using cubic spline extrapolated instead of smoothed values of SWS terms may come on top of the unjustified SWS contributions discussed in section 4. The examples in Fig. 7, furthermore, indicates that the SWS effects, which generate large index differences by their different handling in the near-real time and post-event versions, are equally strong at the Northern and Southern Polar Caps. This result is contrary to the statement of the opposite in pp. 1492-1493 of J&T2011 where SWS-effects are considered negligible for PCS values derived on basis of magnetic data from Vostok on the Antarctic ice cap.

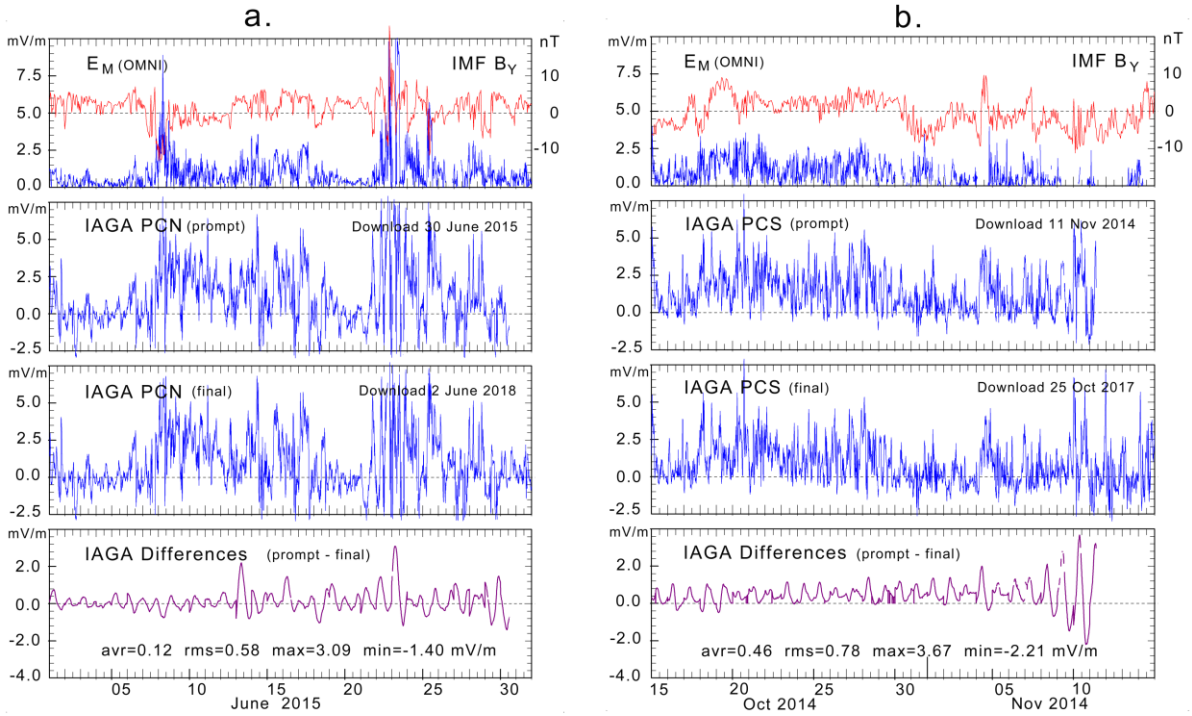

Figure 7. Differences between IAGA-endorsed versions of recorded 15-min values of near-real time and final PCN (left) and PCS (right) indices. (from Stauning, 2018a,c)

In Fig. 7 the real-time values are those seen at the end of the traces termed "prompt". The remaining parts of the prompt traces are "post-event" values where the approximation to the "final" values is thought to be gradually improved as more post-event data become available from dates up to the download time. However, the largest excursions, 3.09 mV/m in PCN and -3.67 mV/m in PCS, are seen at dates prior to the real-time days. Details of the IAGA-endorsed calculation methods are not available for further examination of this issue.

6. Reference levels for PC index calculations in the DMI version.

In the DMI PC index version (Stauning, 2016), the definition of the "solar rotation weighted" (SRW) reference level construction published in Stauning (2011) returns to the statements in Troshichev et al. (2006) with the vector formulation in Eq. 3, and to the methods outlined in

J&T2008. The essential point for the SRW method is deriving the reference level from quiet samples collected at conditions otherwise as close as possible to those prevailing at the day of interest. The factors of primary importance are:

(i) Sample "quietness"

(ii) Separation of samples from QDC date

(iii) Solar wind conditions (particularly IMF B_Y and V_{SW})

(iv) Solar UV and X-ray illumination (based on solar radio flux F10.7 values)

For these factors weight functions are defined. For each hour of the day, observed hourly average values at corresponding hours within an extended interval (±40 days) are multiplied by the relevant weights, added and then divided by the sum of weights to provide the hourly QDC value. Subsequently, the hourly QDC values are smoothed to remove irregular fluctuations and interpolated to provide any more detailed resolution as required.

The weight function for sample quietness is determined from the variability of 1-min data values within the hour much like the technique used by J&T2008. Two parameters are calculated on a vector basis. One is the maximum time derivative used to indicate the smoothness within the sample hour. The other is the average variance to define the slope of data values. Both parameters need to take small values for the hourly sample to be considered "quiet" (flat and featureless display).

For an estimate of further weight functions, the factors of importance were subjected to an autocorrelation analysis vs. separation between the date of interest and the dates of the samples to be included in the construction of the QDC values.

Details of the autocorrelation are provided in Stauning (2011). The main results were, as expected, high autocorrelation values at nearby dates and also high values at dates displaced one full solar rotation of 27.4 days from the day of interest where the solar illumination and the solar wind conditions were similar on a statistical basis to the prevailing conditions. In between, at half a solar rotation, mixed autocorrelation results were found. In some cases a local maximum was seen indicating the occurrence of 4-sector solar wind structures. In most cases the autocorrelation function had a deep minimum at half a solar rotation indicating 2-sector structures. For the solar rotation weighting a squared cosine function was selected to provide unity weights at the QDC date (zero separation), and at dates separated by 27.4 days, and zero weight at half a solar rotation period when the opposite face of the Sun is pointing toward the Earth and the solar wind sector effect, most likely, is in the opposite direction (2-sector structure) or weak (multi-sector structure) (cf. Fig. 6 of Stauning, 2013a).

The final weight factors for sample separation have a central maximum holding 50% of the total weights and two secondary maxima at a solar rotation period (27.4 days) before and after the QDC day holding weights corresponding to 25% of the total weight each. The total span of samples included in the QDC construction is set to ±40 days to encompass all three weight maxima. The separation weight factors are pre-calculated (see Stauning, 2011).

As data are collected the quietness weight factors can be calculated promptly for each hour of recordings along with the hourly averages of each component. The three values are stored. The quietness weight factors are common for the two horizontal components and independent on their representation in (X,Y) or (H,D) coordinates.

Thus, at any time after 80 days of data collection, the relevant final QDC could be calculated for any day more than 40 days in the past. The hourly component averages and their quietness weight factors are fetched from their stored values and their separation weight factors are found from the tabulated values. For each hour of the day, the hourly average component values within ±40 days

are multiplied by the weight factors and summarized. The products of weight factors are summarized. The sum of weighted component hourly average values is divided by the sum of weights to define the hourly QDC value.

The weighting technique allows calculations of real-time QDCs with reduced accuracy by simply ignoring missing samples without changing the calculation scheme. The DMI SRW-method is illustrated in Fig. 7 in a format similar to Fig. 3 with smoothed values of IMF By displayed by the bottom curve (d). The uppermost curve (a) display H_{QDC} values derived by weighting the samples collected at corresponding hours over ±40 days with their "quietness" factors only disregarding the solar rotation weight factors. Curve (b) displays post-event (final) solar rotation-weighted H-QDC values. The next lower curve (c) displays real-time H-QDC values derived by using the SRW calculation scheme but including pre-event samples only (Half solar rotation weighting, HSRW).

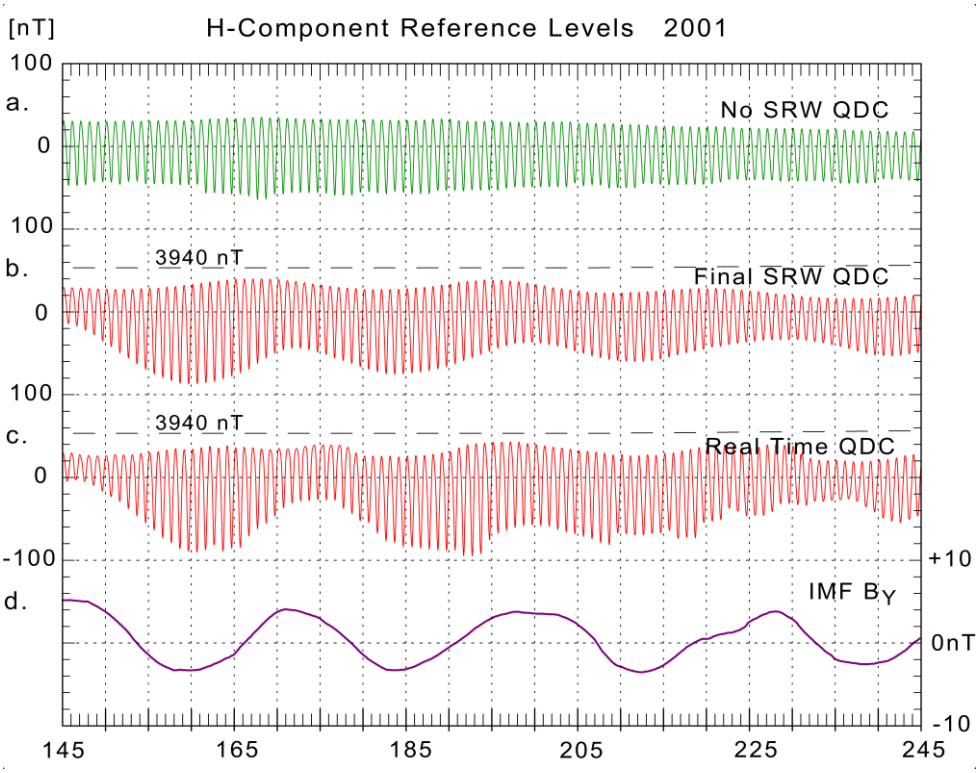

Figure 8. DMI solar rotation weighted (SRW) QDC reference values. (a) QDC with quietness weighting only. (b) Post-event (final) SRW QDC. (c) Real-time (HSRW) QDC values built from past samples only. (d) Smoothed IMF By values.

The upper envelope (night values) of the SRW QDC reference values in curve (b) displays small variations with IMF By while the lower envelope (midday values) and the amplitudes in the daily variation display much stronger variations with IMF B_Y as anticipated from the features seen in Figs. 1 and 2 here (and Fig. 5 of J&T2011). The final QDCs in curve (b) should be compared to the reference levels in curve (c) in Fig. 3. The real-time QDCs in curve (c) in Fig. 8 based on using past data only (0 to -40 days) display more irregular variations than the QDCs based on the full amount (±40 days) as could be expected. However, the real-time reference QDCs in curve (c) in Fig. 8 should be contrasted to the jagged reference levels displayed by curve (e) in Fig. 3. The horizontal dashed lines across the two middle fields present the uppermost level of average H-component values in Fig. 1 (like those drawn in Fig. 3). It is seen that the QDC reference values here – contrary

to the reference levels displayed in Fig. 3 – remain below the uppermost level of statistical mean values for the relevant IMF B_Y ranges.

An example of the relations between post-event (final) and real-time PCN index values is depicted in Fig. 9 using data from the previously selected interval spanning days 145-245 of year 2001.

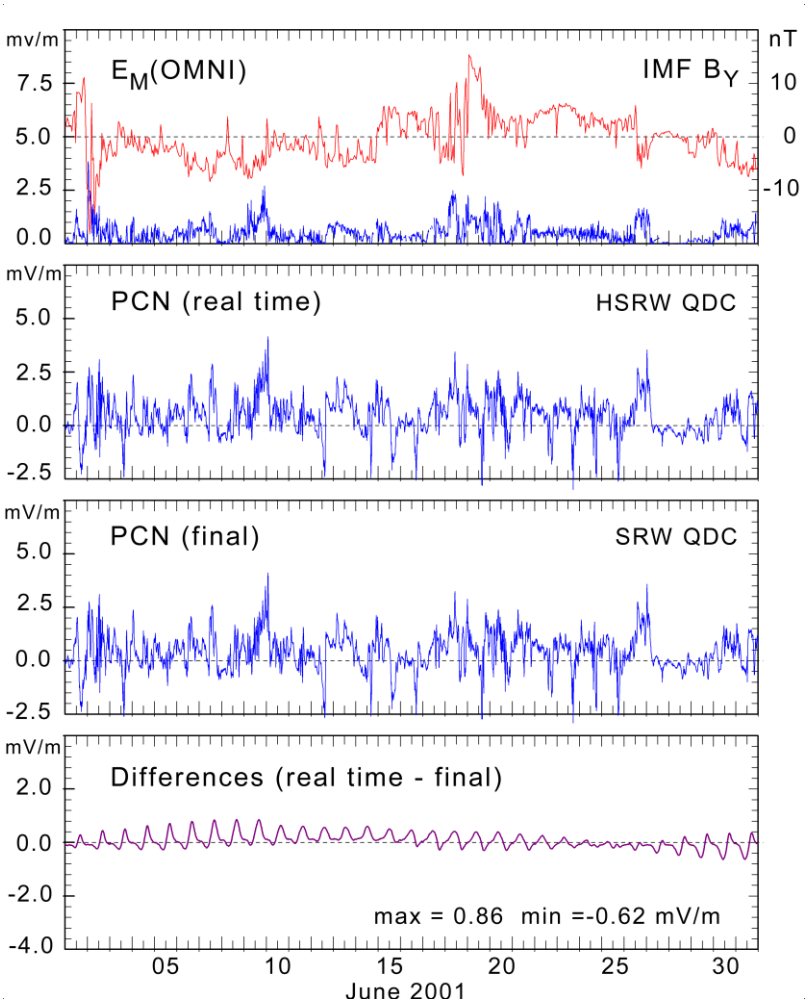

Figure 9. Example of differences between real-time and final PCN values derived by using HSRW QDCs on past data from days -40 to present day only and SRW QDC using the full ±40 days sampling interval.

The differences displayed in the bottom field of Fig. 9 should be contrasted to those displayed at the bottom field of Fig. 6 on the same scale. It is seen that the differences between calculated real-time and post-event PCN index values have been reduced considerably.

In Fig. 7 the prompt index values were downloaded from the web portal http://pcindex.org in near-real time, while the post-event (final) index values were downloaded at a much later time. For further comparisons of IAGA-endorsed methods with the present DMI calculation scheme, Fig. 10 presents for the same dates real-time values of PCN and PCS, which have been constructed from past data using HSRW QDC values on pre-event data only, while the post-event (final) PCN and PCS values have been derived by using the full ±40 days SRW-QDCs.

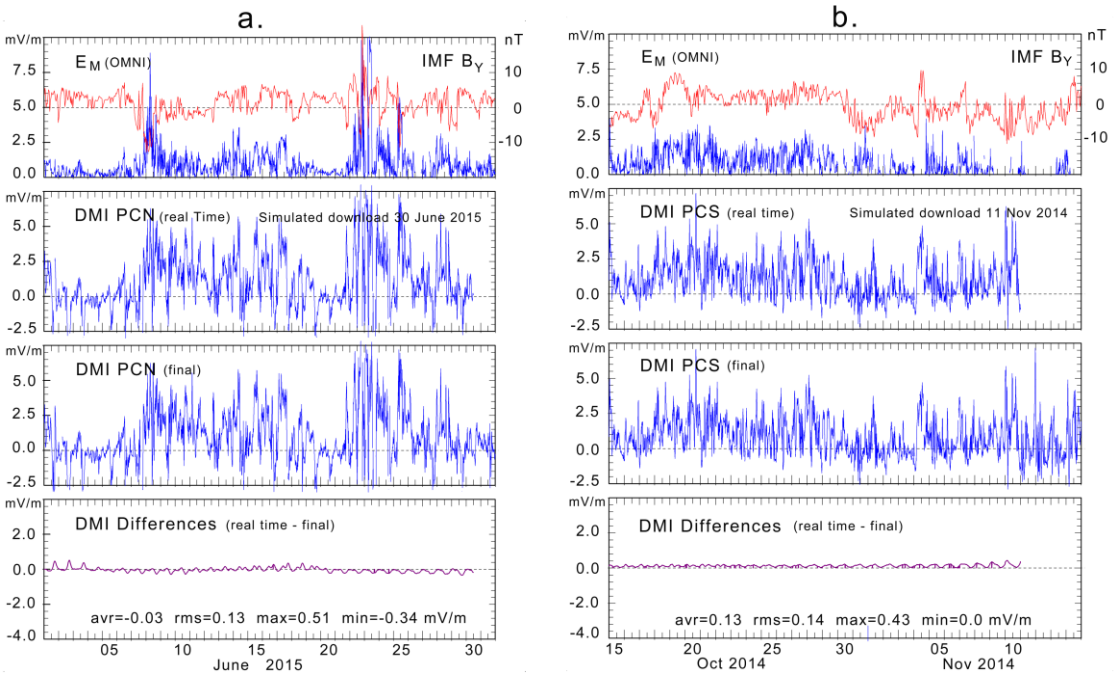

Figure 10. PCN and PCS real-time 15-min values calculated for simulated downloads by using pre-event data only in HSRW QDCs. PCN and PCS final values were calculated by using full SRW QDCs.

Comparing the differences between prompt and post-event PC index values in Fig. 10 with those displayed in Fig. 7 demonstrates the strongly reduced differences obtained by using the HSRW QDC derivation scheme instead of the IAGA-endorsed cubic spline extrapolation method.

An example of both the reduced differences between real-time and final PC index values and the increased robustness to missing data with the DMI method compared to the IAGA-endorsed method is shown in Fig. 11 from Stauning (2018c). The calculations are based on Qaanaaq (THL) data from 2015, which were exposed to irregular recordings at the end of July.

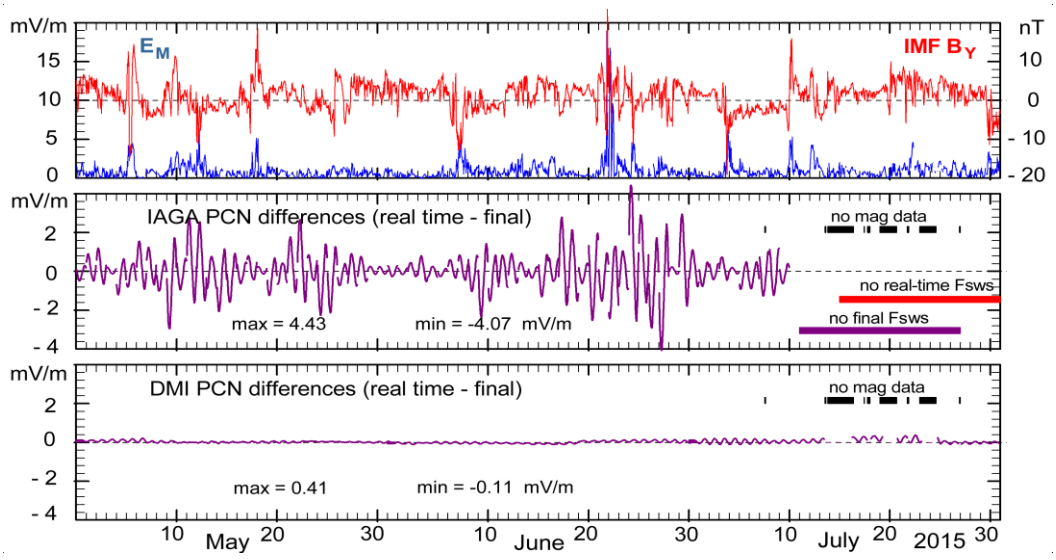

Figure 11. Differences between PCN hourly index values calculated by using real-time and final values of $\mathbf{F}_{SWS}$ in the IAGA-endorsed versions in the middle field and the corresponding differences for the PCN indices in the DMI versions in the bottom field. Intervals of missing values are marked in both lower fields. (from Stauning, 2018c).

PCN index values could not (of course) be calculated where data are missing. The reference levels in the IAGA-endorsed versions are strongly affected by the missing or corrupted median values throughout intervals extending beyond the sections of missing data. The "IAGA PCN differences" of up to more than 4 mV/m in Fig. 11 have been calculated from solar sector terms derived by using the procedure defined in J&T2011.

For Space Weather applications the risk of false PC index values caused by missing data throughout parts of the days, which may cause large displacements of their median values, is probably still more important than missing index data. In an example discussed in Stauning (2018c), where data were made unavailable for 12 hours, the post-event PC index values were changed significantly throughout 13 days centred at the disturbed day. The near-real time indices were changed throughout 8 days after the disturbance by up to 4 mV/m occurring 2 days after the interval of unavailable data. Such amounts may falsely indicate (or hide) strong magnetic storm conditions without warnings.

In Fig. 11, the "DMI PCN differences" between real-time and final PCN index values in the versions based on the SRW techniques remain small (below 0.5 mV/m) and almost unaffected by intervals of missing data. In addition, and of prime importance for the potential use of real-time PC indices in Space Weather monitoring, the SRW-based QDC method, as evident from Fig. 11, is far more robust to data supply irregularities than the cubic spline-based forward extrapolation technique that depends critically on the completeness of data samples.

The application of the DMI methods defined in Stauning (2016), to derive real-time and final PC index values from polar magnetic data assumed currently available, is detailed in the appendix to Stauning (2018c). Relevant magnetic data might be obtained for qualified PCN and PCS calculations from further observatories in the central Polar Regions like Resolute Bay and Dome-C beyond the standard observatories, Qaanaaq and Vostok.

7. Discussions

It should be stressed that the median-based reference levels used in the IAGA-endorsed versions are not quiet levels and thus differ from previous real or verbal definitions of the PC index reference level in publications included those listed as supporting references in the IAGA endorsement documentation written by Matzka (2014) (e.g., Troshichev et al., 2006; Janzhura and Troshichev, 2008; Troshichev, 2011; Janzhura and Troshichev, 2011, Troshichev and Janzhura, 2012a; Troshichev and Janzhura, 2012b). Even at the web portal (http://isgi.unistra.fr) of the International Service of Geomagnetic Indices, ISGI, the PC index definition states (incorrectly) that index values are derived from deviations from the quiet level. The use of median-based reference levels has never been validated in publications and must be considered based on an unjustified postulate originating in Menvielle et al. (2011) and further specified in Janzhura and Troshichev (2011).

A main objection against the IAGA-endorsed reference level construction is the resulting local time variation in IMF B_Y-related effects seen in the H-QDC component in Fig 3 or in the effects on the PCN index values seen in Fig. 4. In both cases the IMF B_Y-related effects contrary to anticipated principles maximize at local night when the observatory is farthest apart from the Cusp region where the IMF By-related effects originate.

It is not, of course, questioned here that the IMF B_Y conditions significantly affect the polar convection patterns and related magnetic variations. However, for the median-based reference level construction, the assumption that slowly varying IMF B_Y levels would not affect geomagnetic disturbance conditions has never been validated and may be incorrect in the complicated interplay

between the IMF B_Y- and B_Z- related effects. A further questionable feature in the reference level derivation method is the implied assumption that SWS terms calculated from daily median values could be applied to remove solar wind sector effects throughout the whole day disregarding the variations in the IMF B_Y–related effects with the varying observatory position in the polar cap. The real IMF B_Y-related SWS effects on the PC indices could even be opposite of the constructed effects resulting from using reference level values derived by the median-based methods whether in the post-event or in the real-time version.

The example PCN calculations displayed in Fig. 4 were based on the case presented in J&T2011 with a smoothed IMF B_Y value of 4 nT, which is not uncommon. Unjustified SWS contributions of 3-4 mV/m could be expected for the stronger cases (larger IMF B_Y). Such magnitudes are around twice the onset level of around 2 mV/m for magnetic storm or substorm activity (Troshichev et al., 2014), which definitely makes the IAGA-endorsed "final" PCN indices unsuitable for scientific applications.

For the PCS indices, corresponding problems with the post-event reference levels may exist in spite of the statement in p. 1492-1493 of J&T2011 that SWS effects are negligible at Vostok on the Antarctic ice cap. It has not been possible to obtain a description of the present PCS calculation methods from the index provider (AARI) or from the index publisher (ISGI) for further examination of this issue.

For the real-time PCN and PCS indices, the excessive excursions in the cubic-spline extrapolated reference levels may generate unfounded differences between near-real time and post-event index values of more than 4 mV/m. Such excursions with magnitudes at magnetic storm levels make the near-real time IAGA-recommended PC indices unreliable and thus unsuitable for Space Weather monitoring and related research. Their strong vulnerability to intervals of incomplete data with the maximum adverse effects appearing two days after the occurrence of data irregularities is an additional invalidating feature to be considered.

It has not been possible to obtain descriptions of the real-time PCN and PCS calculation methods from the index provider (AARI) or from the index publisher (ISGI). It has also not been possible to obtain archived recordings of near-real time PCN and PCS indices provided to the community through the AARI web portal http://pcindex.org and the ISGI web site http://isgi.unistra.fr .

The concerns over the inconsistent index derivation methods and lack of documentation have been forwarded to IAGA Executive Committee, Index Task Force and Working Group representatives and to the PC index providers at AARI and DTU Space with suggestions for thorough analyses of PC index calculation methods. The specific concerns have not been responded to and the suggestions for further analyses of the index derivation methods have been rejected so far.

8. Irregular PCS excursions

The search for unjustified SWS effects in the PC index series has disclosed numerous examples of irregular unjustified PCS excursions. An example from a recent download of PCN and PCS data from 15-18 December 2011 is displayed in Fig.12 (For the review process, further examples from still more recent downloads (27 Jan 2020) are shown in appendix A2.)

Fig. 12 displays in addition corresponding PCN and PCS values derived by the DMI index procedure (Stauning, 2016). The display of PCS index values based on Vostok data is supplemented by PCS index values derived from Dome-C (DMC) magnetic data, which are of very good quality. The Vostok and Dome-C data generate nearly identical PCS values and indicate very low disturbance levels. The interval is very quiet (Kp values between 0 and 1) which is also evident from the PCN data in both versions.

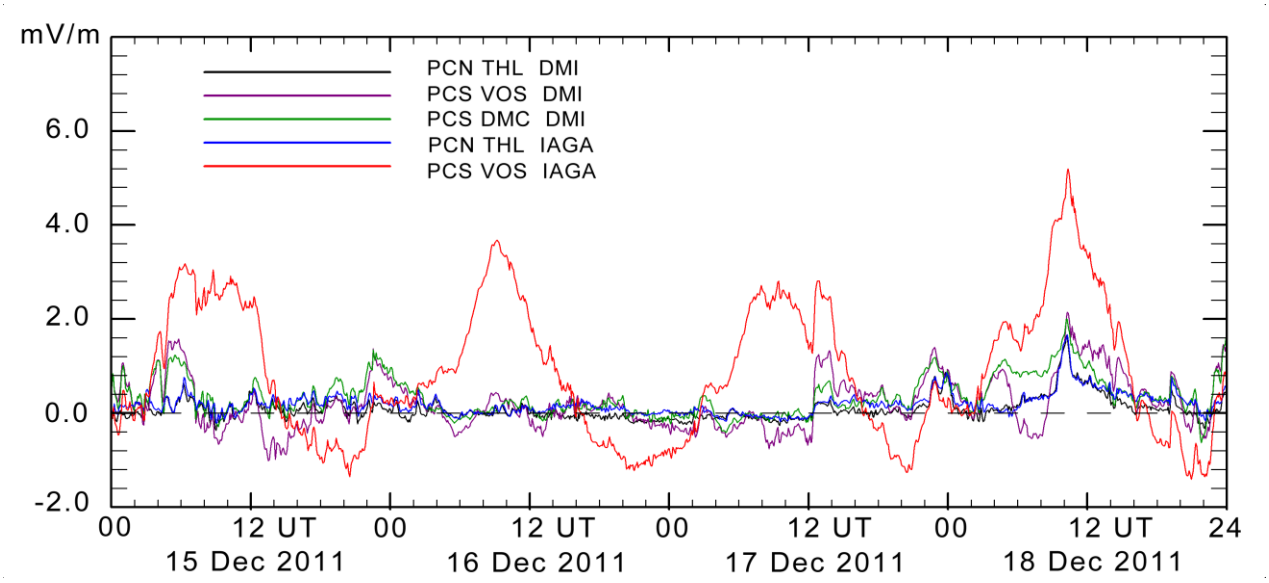

Figure 12. Display of published PCN (blue line) and PCS (red) values from 15-18 December 2011. PCN (black) from Qaanaaq data, PCS from Vostok (magenta) and Dome-C (green) data derived by a different method (DMI, Stauning, 2016) have been added to the diagram.

It is easy to see that the published Vostok PCS data have unjustified daily variations between -1.5 and up to +4.0 mV/m (a level indicative of strong magnetic storm conditions). The additional top of 1 mV/m bringing the PCS value up to 5.0 mV/m at 11 UT on 18 December is probably a real event. The Vostok magnetic data supplied from INTERMAGNET are final values.

The excessive PCS variations are probably not caused by implementation of the SWS-related reference level construction but may have resided in the PCS index values calculated at AARI throughout the years and brought to attention now by the recent examination of PCS data for SWS effects. The PCS index failure is mentioned here to underline the point that PC index series need careful monitoring and evaluation of index quality, which is apparently not implemented.

Information on the problem in the PCS index series distributed from ISGI (http://isgi.unistra.fr) and the AARI index web portal (http://pcindex.org) was published in Stauning (2018b) and also sent directly to the index providers and to ISGI and IAGA representatives in 2018. Their only reaction – so far – has been to state that the published PCS index data are just provisional values to be applied to scientific works at users own risk (communication from IAGA Executive Committee, 21 May 2018).

Conclusions.

- The Polar Cap indices in their real-time versions have the potential to become very important tools for Space Weather monitoring and forecasts and in their final versions important for Space Weather-related research. However, the presently published PCN and PCS index series are considered invalid.

- The published series of (nominally) final PCN index values calculated by the methods endorsed by IAGA may include unjustified contributions of up to 3-4 mV/m just due to the handling of IMF B_Y-related solar wind sector effects in the reference level construction. An example case gave unjustified contributions of up to 2.5 mV/m (magnetic storm level) to PCN index values. Such unjustified contributions are considered to make the “final” PCN index series invalid.

- The series of near-real time PCN and PCS index values calculated by the methods endorsed by IAGA may display considerable differences with respect to their corresponding post-event values. An example case using the referenced calculation procedures to the letter gave differences of up to 2.8 mV/m for a moderate event. Further examples of calculations of effects have given differences of more than 4 mV/m. At occasional downloads of near-real time index values and comparison to later downloads of final values, differences of up to 3.7 mV/m have been documented in cases not particularly extreme.

- The IAGA-endorsed near-real time index calculation method based on cubic spline extrapolation of past median values is extremely vulnerable to irregularities in the data supply. An example of 12 hours of missing data gave unfounded excursions of up to 4 mV/m two days later. Such excursions may falsely indicate (or hide) strong magnetic storm conditions and are considered to make the IAGA-recommended near-real time indices highly unreliable and thus unsuitable for Space Weather applications.

- The provisional PCS index series, which is not approved by IAGA but still made available from ISGI and used in the scientific community, displays unexplained erroneous excursions of up to 4 mV/m in the recorded examples shown here. Final magnetic data were available for the index examples and the IAGA-endorsed calculation methods were probably used. Similar or even larger undetected excursions are possible. The example underlines the need for careful examination of index quality in the published PC index series.

- It is suggested that IAGA should initiate a careful evaluation of present index series and index derivation methods and ensure that full documentation of the presently applied index calculation procedures is made available in agreement with its *Criteria for endorsement of indices by IAGA, sec.2* (2009). Presently, there is no available documentation of present PCS index derivation procedures or of the near-real time PCN and PCS calculation methods.

- On basis of the problems reported here, IAGA might consider encouraging developments of improved PC index calculation methods. Alternative more accurate and reliable methods are available.

Data availability:

Near real-time (prompt) PC index values and archived PCN and PCS index series derived by the IAGA-endorsed procedures are available through AARI and ISGI web sites. Archived PCN and PCS data used in the paper were downloaded from http://pcindex.org on 15 November 2019 unless otherwise noted. The web site, furthermore, holds PCN and PCS index coefficients, whereas QDC and SWS values are not included. The web site includes the document “Polar Cap (PC) Index” (Troshichev, 2011).

It is presently not known (in spite of requests) whether the near real-time PC index suppliers (AARI and ISGI) retain copies of the published values. If not available from the index suppliers, then values of occasionally downloaded values held by the author could be delivered, for instance, in their original (zip-encoded) formats to a data repository or included in a data supplement.

Geomagnetic data from Qaanaaq, Vostok, and Dome-C were supplied from the INTERMAGNET data service web portal at http://intermagnet.org.

The observatory in Qaanaaq is managed by the Danish Meteorological Institute, while the magnetometer there is operated by DTU Space, Denmark. The Vostok observatory is operated by the Arctic and Antarctic Research Institute in St. Petersburg, Russia. The Dome-C observatory is

managed by Ecole et Observatoire des Sciences de la Terre (France) and Istituto Nazionale di Geofisica e Vulcanologia (Italy).

The "DMI" PC index version is documented in the report SR-16-22 (Stauning, 2016) available at the web site: http://www.dmi.dk/fileadmin/user_upload/Rapporter/TR/2016/SR-16-22-PCindex.pdf

Acknowledgments. The staffs at the observatories in Qaanaaq (Thule), Vostok, and Dome-C, and their supporting institutes are gratefully acknowledged for providing high-quality geomagnetic data for this study. The efficient provision of geomagnetic data from the INTERMAGNET data service centre, and the excellent performance of the PC index portals are greatly appreciated. The author gratefully acknowledges the good collaboration and many rewarding discussions in the past with Drs. O. A. Troshichev and A. S. Janzhura at the Arctic and Antarctic Research Institute in St. Petersburg, Russia.

References

Chun, F. K., Knipp, D. J., McHarg, M. G.., Lu, G., Emery, B. A., Vennerstrøm, S., Troshichev, O. A. (1999), Polar cap index as a proxy for hemispheric Joule heating, *Geophys. Res. Lett.*, *26* , 1101-1104. https://doi.org/10.1029/1999GL900196

Chun, F.K., Knipp, D. J., McHarg, M. G., Lacey, J. R., Lu, G., and Emery, B. A. (2002), Joule heating patterns as a function of polar cap index, *J. Geophys. Res.*, *107* (A7), https://doi.org/10.1029/2001JA000246 .

Iijima, T., Potemra, T.A. (1976). Field-aligned currents in the Cusp observed by Triad, *Journal of Geophysical Research*, 81, 5971-5979. https://doi.org/10.1029/JA081i034p05971

IAGA Resolution no. 3 (2013): http://www.iaga-aiga.org/resolutions.

IAGA Index endorsement criteria (2009): https://www.ngdc.noaa.gov/IAGA/vdat/GeomagneticIndices/Criteria_for_Endorsement.pdf

Huang, C.-S. (2005), Variations of polar cap index in response to solar wind changes and magnetospheric substorms, *J. Geophys. Res.*, 110, A01203, https://doi.org/10.1029/2004JA010616 .

Janzhura, A. S., Troshichev, O. A. (2008). Determination of the running quiet daily geomagnetic variation. *Journal of Atmospheric and Solar-Terrestrial Physics*, 70, 962–972. https://doi.org/10.1016/j.jastp.2007.11.004 .

Janzhura, A. S., Troshichev, O. A. (2011). Identification of the IMF sector structure in near-real time by ground magnetic data. *Annales Geophysicae*, 29, 1491-1500. https://doi.org/10.5194/angeo-29-1491-2011 .

Janzhura, A. S., Troshichev, O. A., Stauning, P. (2007). Unified PC indices: Relation to the isolated magnetic substorms. *Journal of Geophysical Research*, 112, A09207. https://doi.org/10.1029/2006JA012132 .

Kan, J. R., Lee, L. C. (1979). Energy coupling function and solar wind-magnetosphere dynamo. *Geophysical Research Letter*, 6 (7)**,** 577– 580. https://doi.org/10.1029/GL006i007p00577 .

Liou, K., Carbary, J. F., Newell, P. T., Meng, C. I., and Rasmussen, O. (2003). Correlation of auroral power with the polar index, *J. Geophys. Res.*, *108* (A3), 1108, https://doi.org/10.1029/2002JA009556 .

695 Matzka, J. (2014). PC_index_description_main_document_incl_Appendix_A.pdf. Available at
696 DTU Space web portal: ftp://ftp.space.dtu.dk/WDC/indices/pcn/

697 Menvielle, M., Iyemori, T., Marchaudon, A., Nosé, M. 2010. Geomagnetic Indices. Ch.8 in: M.
698 Mandea, M. Korte (eds), *Geomagnetic Observations and Models*, IAGA Special Sopron Book
699 Series 5, 2011. pp.183-228. https://doi.org/10.1007/978-90-481-9858-0_8

700 Nagatsuma T. (2002). Saturation of polar cap potential by intense solar wind electric fields,
701 *Geophys. Res. Let.*, *29*, (10), 621. https://doi.org/10.1029/2001GL014202

702 Nielsen, J. B. and Willer, A. N. (2019). Restructuring and harmonizing the code used to calculate
703 the Definitive Polar Cap Index, *Report from DTU Space*. https://tinyurl.com/sx3g5t5

704 Ridley A.J. and Kihn, E. A. (2004). Polar cap index comparisons with AMIE cross polar cap
705 potential, electric field, and polar cap area, *Geophys. Res. Lett.*, *31*, L07801,
706 https://doi.org/10.1029/2003GL019113 .

707 Stauning, P. (2011). Determination of the quiet daily geomagnetic variations for polar regions, *J.*
708 *Atmos. Solar-Terr. Phys.*, https://doi.org/10.1016/j.jastp.2011.07.004 .

709 Stauning, P. (2012). The Polar Cap PC Indices: Relations to Solar Wind and Global Disturbances,
710 Exploring the Solar Wind, Marian Lazar (Ed.). *InTech Publ.*. ISBN: 978-953-51-0339-4.
711 https://doi.org/10.5772/37359

712 Stauning, P. (2013a). The Polar Cap index: A critical review of methods and a new approach, *J.*
713 *Geophys. Res. Space Physics*, 118, 5021-5038. https://doi.org/10.1002/jgra.50462

714 Stauning, P. (2013b). Comments on quiet daily variation derivation in "Identification of the IMF
715 sector structure in near-real time by ground magnetic data" by Janzhura and Troshichev (2011).
716 *Annales Geophysicae*, 31, 1221-1225. https://doi.org/10.5194/angeo-31-1221-2013 .

717 Stauning P. (2013c). Power grid disturbances and polar cap index during geomagnetic storms, *J*
718 *Space Weather Space Clim*. ***3***: A22. https://doi.org/10.1051/swsc/2013044 .

719 Stauning, P. (2015). A critical note on the IAGA-endorsed Polar Cap index procedure: effects of
720 solar wind sector structure and reverse polar convection. *Annales Geophysicae*, 33**,** 1443-1455.
721 https://doi.org/10.5194/angeo-33-1443-2015 .

722 Stauning, P. (2016). The Polar Cap (PC) Index.: Derivation Procedures and Quality Control. *DMI*
723 *Scientific Report SR-16-22*. Available at:
724 https://www.dmi.dk/fileadmin/user_upload/Rapporter/TR/2016/SR-16-22-PCindex.pdf .

725 Stauning, P. (2018a). A critical note on the IAGA-endorsed Polar Cap (PC) indices: excessive
726 excursions in the real-time index values. *Annales Geophysicae*, 36, 621–631.
727 https://doi.org/10.5194/angeo-36-621-2018 .

728 Stauning, P. (2018b): Multi-station basis for Polar Cap (PC) indices: ensuring credibility and
729 operational reliability. *Journal of Space Weather and Space Climate*, 8, A07.
730 https://doi.org/10.1051/swsc/2017036 .

731 Stauning, P. (2018c). Reliable Polar Cap (PC) indices for space weather monitoring and forecast,
732 *Journal of Space Weather and Space Climate*, 8**,** A49. https://doi.org/10.1051/swsc/2018031

733 Stauning, P. (2020). Using PC indices to predict violent GIC events threatening power grids.
734 *Journal of Space Weather and Space Climate*. https://doi.org/10.1051/swsc/202004 .

735 Stauning, P., Troshichev, O. A., and Janzhura, A. S. (2008). The Polar Cap (PC) index: Relations to
736 solar wind parameters and global activity level, *J. Atmos. Solar-Terr. Phys.*,
737 https://doi.org/10.1016/j.jastp.2008.09.028 .

738 Troshichev, O. A. (2011). Polar Cap (PC) Index. Available at: http://pcindex.org (see Supported
739 materials).Troshichev, O. A. and Andrezen, V. G. (1985). The relationship between
740 interplanetary quantities and magnetic activity in the southern polar cap. *Journal of Planetary*
741 *and Space Science*, 33, 415-419. https://doi.org/10.1016/0032-0633(85)90086-8

742 Troshichev, O. A. and Janzhura, A. S. (2012a). Physical implications of discrepancy between
743 summer and winter PC indices observed in the course of magnetospheric substorms. *Advances in*
744 *Space Research*, 50 (1), 77-84. https://doi.org/10.1016/j.asr.2012.03.017

745 Troshichev, O. A. and Janzhura, A. S. (2012b). Space Weather monitoring by ground-based means,
746 *Springer Praxis Books*. Heidelberg. https://doi.org/10.1007/978-3-642-16803-1 .

747 Troshichev, A. O. and Lukianova, R. Y. (2002). Relation of PC index to the solar wind parameters
748 and substorm activity in time of magnetic storms, J. Atmos. Solar-Terr. Phys., 64, 585.
749 https://doi.org/10.1016/S1364-6826(02)00016-0 .

750 Troshichev, O. A., Sormakov, D. A. (2017). PC index as a proxy of the solar wind energy that entered into the
751 Magnetosphere: 3. Development of magnetic storms, *J. Atmos. Solar-Terr. Phys.*
752 https://doi.org/10.1016/j.jastp.2017.10.012

753 Troshichev, O. A., Andrezen, V. G., Vennerstrøm, S., Friis-Christensen, E. (1988). Magnetic activity in the polar cap –
754 A new index. *Journal of Planetary and Space Sciences*, 36(11), 1095-1102. https://doi.org/10.1016/0032-
755 0633(88)90063-3

756 Troshichev, O. A., Janzhura, A. S., Stauning, P. (2006). Unified PCN and PCS indices: method of
757 calculation, physical sense and dependence on the IMF azimuthal and northward components.
758 *Journal of Geophysical Research*, 111, A05208. https://doi.org/10.1029/2005JA011402 . (note
759 correction in Troshichev et al., 2009)

760 Troshichev, O. A., Janzhura, A. S., Stauning, P. (2009). Correction to "Unified PCN and PCS
761 indices: Method of calculation, physical sense, and dependence on the IMF azimuthal and
762 northward components", *Journal of Geophysical Research*, 114, A11202.
763 https://doi.org/10.1029/2009JA014937 .

764 Troshichev, A. O., Lukianova, R. Y., Papitashvili, V. O., Rich, F. J. and Rasmussen, O. (2000).
765 Polar Cap index (PC) as a proxy for ionospheric electric field in the near-pole region, Geophys.
766 Res. Lett., 27, 3809. https://doi.org/10.1029/2000GL003756

767 Troshichev, O. A. , Podorozhkina, N. A., Sormakov, D. A., Janzhura, A. S. (2014). PC index as a
768 proxy of the solar wind energy that entered into the magnetosphere: 1. Development of magnetic
769 substorms. *Journal of Geophysical Research, Space Physics*, 119.
770 https://doi.org/10.1002/2014JA019940 .

771 Vassiliadis, D., V. Angelopoulos, D. N. Baker, A. J. Klimas (1996), The relation between the
772 northern polar cap and auroral electrojet geomagnetic indices in the wintertime, *Geophys. Res.*
773 *Lett.*, *23*, 2781. https://doi.org/10.1029/96GL02575 .

774 Vennerstrøm, S. (1991). The geomagnetic activity index PC, PhD Thesis, Scientific Report 91-3,
775 Danish Meteorological Institute, 105 pp.
776 https://www.dmi.dk/fileadmin/user_upload/Rapporter/SR/1991/sr91-3.pdf

777 Vennerstrøm, S., Friis-Christensen, E., Troshichev, O. A., Andrezen, V. G. (1991). Comparison
778 between the polar cap index PC and the auroral electrojet indices AE, AL and AU, *J. Geophys.*
779 *Res.*, *96*, 101. https://doi.org/10.1029/90JA01975

780 Wilhjelm, J., Friis-Christensen, E., Potemra, T. A. (1972). The relationship between ionospheric
781 and field-aligned currents in the dayside cusp, J. Geophys. Res. 83, 5586.
782 https://doi.org/10.1029/JA083iA12p05586

Funding:

No external funding was involved in this work.

Conflict of interest:

I have no conflict of interest

Appendix A1 (This appendix is intended for the review process only.)

A1-1. Reference level. The only published description of real-time versions of the Polar Cap (PC) indices, PCN and PCS, is found in Janzhura and Troshichev (2011): Identification of the IMF sector structure in near-real time by ground magnetic data (J&T2011) (and its replicate in Troshichev and Janzhura, 2012, T&J2012). The publication holds (p.1496) a step-by-step procedure for the calculation of IMF By-related solar wind sector (SWS or SS) terms by forward cubic spline-based extrapolation of past median values. The SS terms are used in the derivation of reference levels for measuring magnetic variations. In their work, in spite of statements to the opposite, there are no examples of near-real time data or values derived from using the specified real-time method.

The present note provides copies of figures of J&T2011 (T&J2012), and displays corresponding figures based on post-event as well as real-time data processing at DMI.

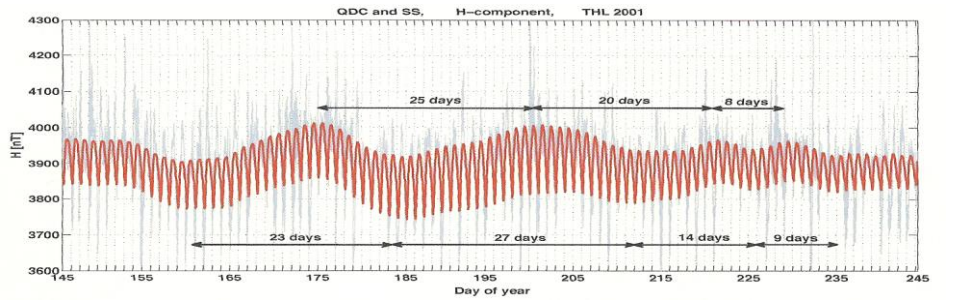

Figure 4.10 The actual variation of 1-min values of the geomagnetic *H* component at Thule station in the summer season of 2001 (blue thin line) and superposed quiet daily curve (QDC) characterizing the daily variation of the quiet geomagnetic field (red thick line).

Fig. A1-1. PCN reference level (red) superimposed on recorded H-component data. From Fig. 1 of J&T2011, reproduced here in colour from Fig. 4.10 of T&J2012

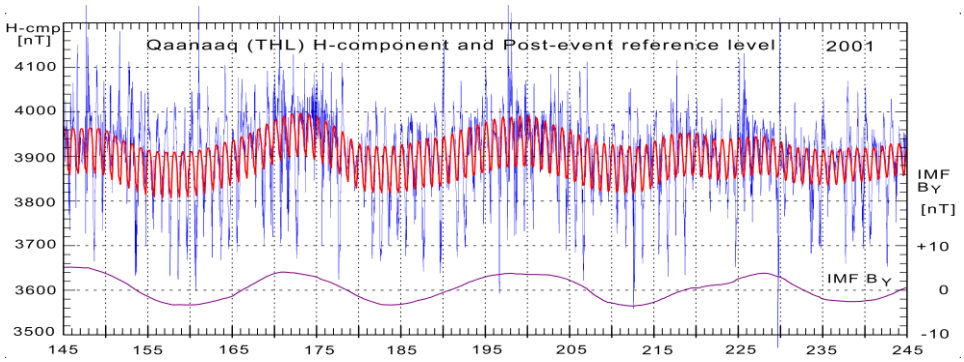

Fig. A1-2. PCN post-event (final) reference level values (red line) supplied from DTU Space superimposed on recorded H-component data. IMF By values added.

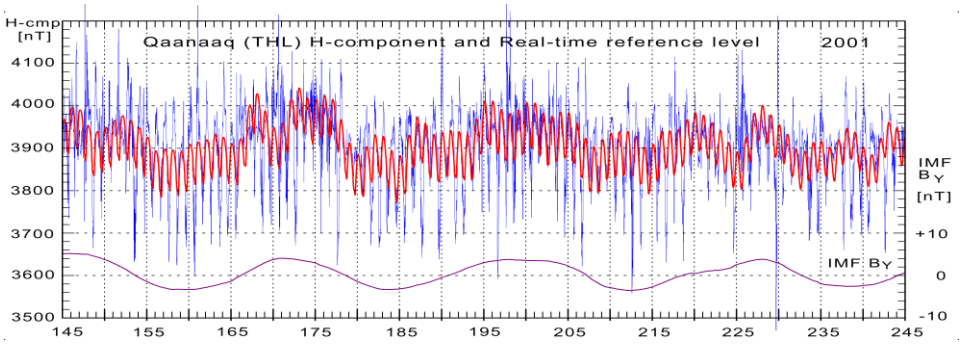

Fig. A1-3. PCN real-time reference level (red) derived by using J&T2011 procedure to the letter. Recorded H-component data. IMF By values added.

The close similarity of the reference level (red line) in Fig.A1-1 with that of Fig.A1-2 and the strong difference with respect to the real-time reference level in Fig.A1-3 implies that the "QDC" in Fig.A1-1 was actually derived by post-event (final) calculation methods like those used for Fig.A1-2.

A1-2. Solar Wind Sector (SS) term.

The IMF By-related solar wind sector effects on the convection patterns generate changes in the PC index response to the merging electric fields. A solar wind sector term was first suggested by Menvielle et al. (2011) and implemented in the derivation of PC index reference levels by Janzhura and Troshichev (2011) (replicated in T&J2012). For post-event processing the SS terms were derived as the smoothed average values of 7 days daily median values. For real-time processing, the SS terms are derived from cubic spline-based extrapolation of past median values according to J&T2011 (T&J2012). However, in spite of the explicit statement in p. 1496 of J&T2011 assuring that the illustration of the SS term in their Fig. 6 (Fig. 4.15 in T&J2012) is based on using the real-time procedure, the figure actually presents values derived by the post-event method (7-days smoothed average daily medians).

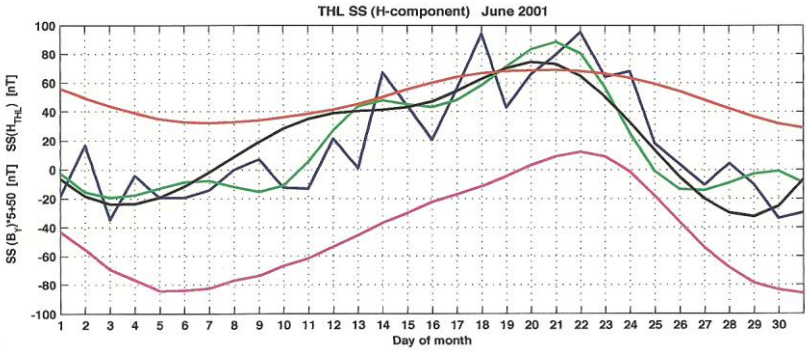

Fig. A1-4. THL H-component. 1-day (blue), 3-days (green) and 5-days (black) median values. H_{SS} terms in magenta line on scale shifted 50 nT downward for clarity. Smoothed IMF By multiplied by 5 and shifted 50 nT upward. (From Fig. 6 of J&T2011. Here copied from Fig. 4.15 of T&J2012)

Figure 4.15 Behavior of the median values of the magnetic *H* component at Thule station during June months of 1998 (a) and 2001 (b) for intervals with duration of 1 day (blue line), 3 days (green line), and 5 days (black line). The red line shows the variation of the IMF B_Y component, derived from spacecraft measurements. The magenta line shows the variation reconstructed from geomagnetic *H* component. To be clearly demonstrated the actual B_Y values were multiplied by a five and were shifted by 50 nT to a higher position, whereas the curve of reconstructed *H* component was shifted by 50 nT to a lower position.

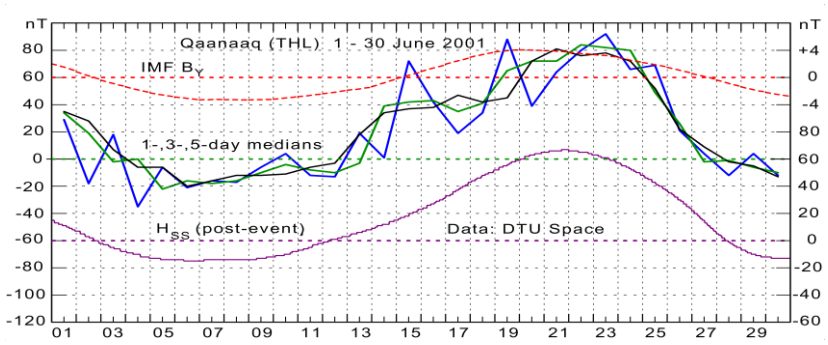

Fig. A1-5. THL 1-, 3-, 5-day medians on left scale. Post-event H_{SS} terms are displayed in magenta line on lower right scale. Data were supplied from DTU Space. IMF By values added on upper right scale (OMNI).

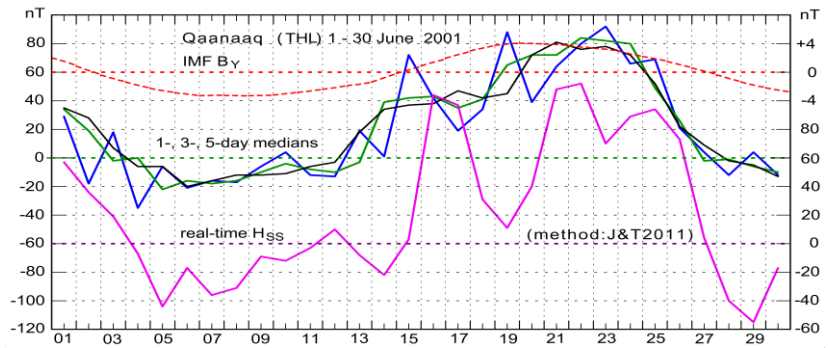

Fig. A1-6. THL 1-, 3-, 5-day medians on left scale. Real-time H_{SS} terms in magenta line on lower right scale. H_{SS} values were calculated by following the procedure in J&T2011 to the letter. IMF By added on upper right scale

The similarity between the H_{SS} curves in Figs.A1-4 and A1-5 and the large difference with respect to the real-time H_{SS} values in Fig.A1-6 implies that the display in Fig. 6 of J&T2011 (Fig. 4.15 of T&J2012), contrary to the statement in p. 1496, was actually generated from using post-event calculations.

A1-3. H-component and SS terms.

Fig. 7 in J&T2011 (Fig. 4.16 in T&J2012) displays the H-component recorded at Qaanaaq (THL) throughout year 2001. The IMF B_Y-related H_{SS} values have been superimposed on the recordings. The black asterisks are supposed to present real-time, the red asterisks present post-event values.

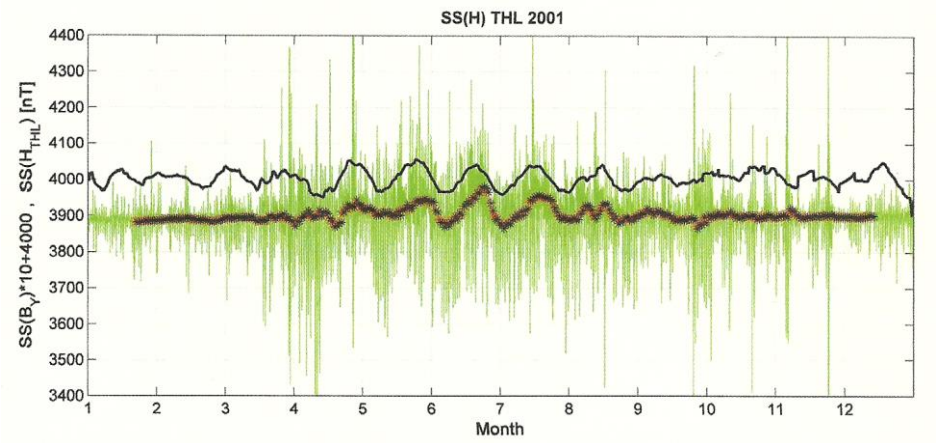

Fig. A1-7. Presentation of one year's THL H-component data (green line) with superimposed real-time (black), and post-event H_{SS} values (red asterisks). IMF By values added (black line). From Fig. 7 of J&T2011. Here copied from Fig.4.16 of T&J2012

Figure 4.16 The SS effects derived in the *H* component observed at station Thule in 1998 (a) and 2001 (b). The actual variation of the ground *H* component is shown by a green line, whereas black asterisks present the SS structure obtained by the extrapolation procedure when all data are available until the examined day (n=1); and red asterisks present the interpolated SS structure derived under the condition that the examined day is in the middle of the gap in the time interval. The actual variation of the IMF B_y component values measured by ACE spacecraft were multiplied by a ten and were shifted by 4000nT to a higher position (thin black line).

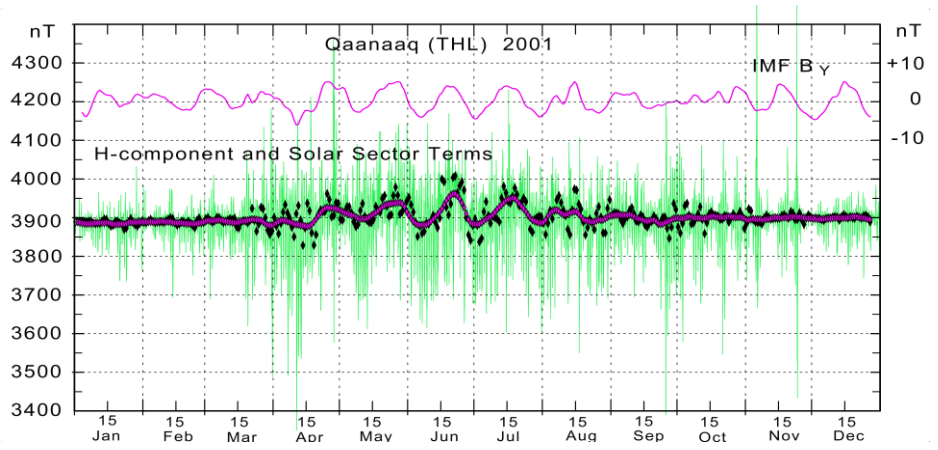

Fig. A1-8. THL H-component data with superimposed real-time (black), and post-event (red diamonds) values of H_{SS}. Note the large scatter of the real-time (black) diamonds. IMF By values added.(red line) on upper right scale.

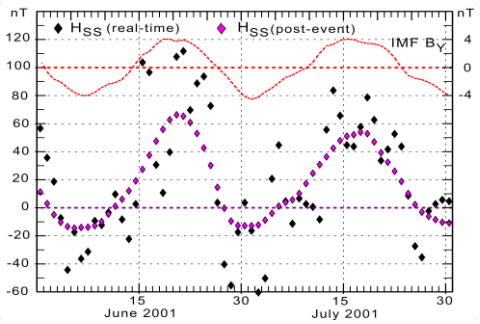

Fig. A1-9. Detailed plot of June-July section of Fig. A8. Black diamonds present real-time H_{SWS} values derived by using the J&T2011 procedure (p.1496) to the letter. The magenta diamonds present post-event (final) H_{SS} values supplied from DTU Space. They represent daily median H-component values averaged and smoothed over 7 days at a time.
IMF B_Y values displayed in red line on right scale.

It is evident from Figs.A1-8 and A1-9 that the real-time and post-event methods generate quite different values of the IMF B_Y-related solar wind sector terms, H_{SS}. The red set of asterisks in Fig. A1-7, no doubt, present post-event values, while the black set, against the statement in the caption, could not present real-time values.

A1-4. SS term vs. IMF By

From the post-event processing it appears that the H- and D-solar wind sector terms are highly correlated with the daily mean IMF B_Y values. Thus, they could be used to estimate past IMF B_Y levels and signs with good probability. However, according to the title and abstract of the publication, "Identification of the IMF sector structure in near-real time by ground magnetic data", the real-time and not the post-event option is the target.

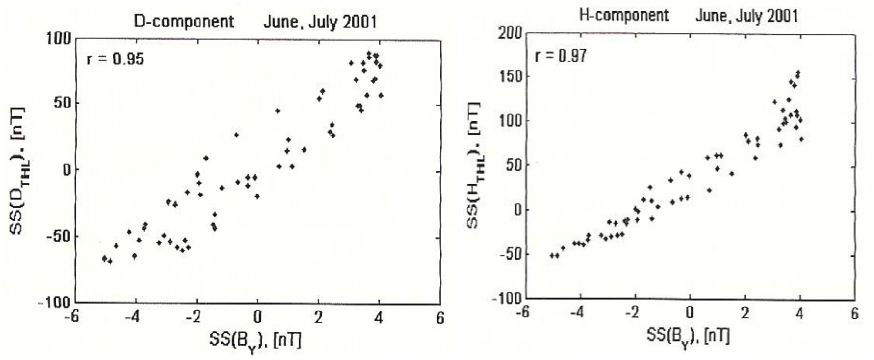

Figure 4.17 Relationship between the sector structure magnitudes derived by satellite-based and ground-based sets of magnetic data for summer months of 1998 (upper row) and 1991 (lower row). Geomagnetic D (left column) and H (right column) components at the Thule stations were analyzed.

Fig. A1-10. Fig. 8b from J&T2011 (Fig.4.17 from T&J2012).Relations between daily average IMF B_Y values and solar wind sector D_{SS} and H_{SS} values. H_{SS} scale values are too large by a factor 2 (cf. their Fig. 4.16).

Year 1991 should be 2001.

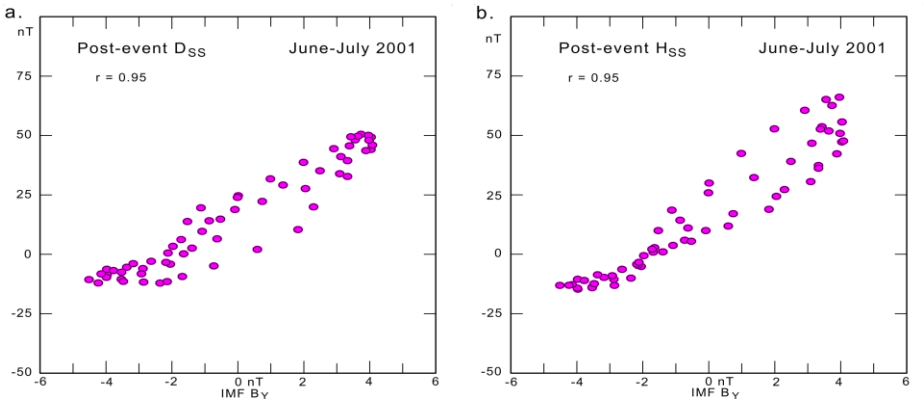

Fig. A1-11. Display of post-event (final) solar wind sector terms, H_{SS}, supplied from DTU Space vs. daily average IMF B_Y values. Note the H_{SS} scales differ by factor 2 from those of Fig. A10, i.e., Fig. 8 of J&T2011 (Fig. 4.17 of T&J2012).

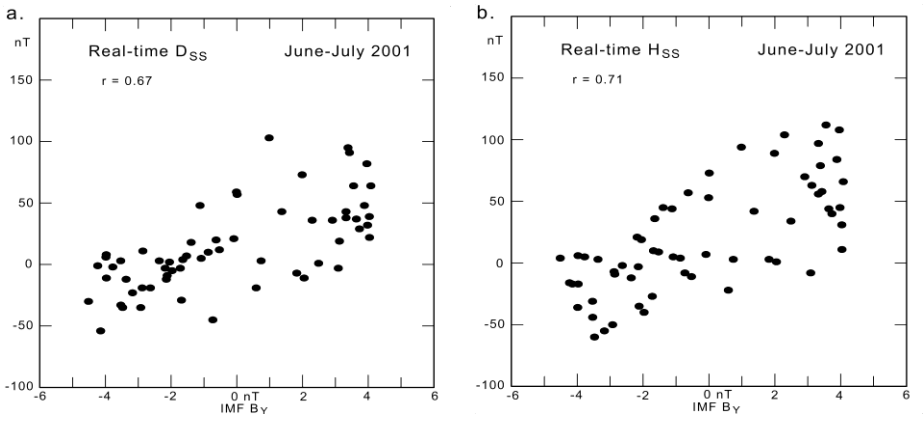

Fig. A1-12. Display of real-time solar wind sector terms, H_{SS}, calculated by using the procedure in J&T2011, p.1496, to the letter, plotted vs. daily average IMF B_Y values.

Contrary to the D_{SS} and H_{SS} solar wind sector terms derived by post-event calculations displayed in Figs. A1-10 and A1-11, the corresponding solar wind sector terms generated by using real-time processing are less well correlated with the daily average IMF B_Y values. The relation displayed by the scattered values in Fig. A1-12 could hardly be used to determine the actual IMF By magnitude level and sign with certainty.

867

868 **A1-5. Appendix A1 summary.**

869 With the title of the publication, Janzhura and Troshichev (2011) (or its replica in section 4.4 of Troshichev
870 and Janzhura, 2012): "*Identification of the IMF sector structure in near-real time by ground magnetic data*"
871 and their abstract: "*A method is proposed to determine in near-real time the interplanetary magnetic field*
872 *(IMF) sector structure effect on geomagnetic data from polar cap stations*", the publication could be
873 expected to present examples of near-real time data or derived results.

874 The publication presents the IMF By-related solar wind sector effects by introducing solar wind sector terms
875 (D_{SS} and H_{SS}) derived from the daily median component values averaged throughout 7 days with the day of
876 interest at the middle. These solar wind sector terms are used for calculations of the reference level from
877 which the polar magnetic disturbances used to generate the polar cap (PC) indices are derived (Matzka,
878 2014).

879 The post-event method was extended to generate solar wind sector terms in near-real time by cubic spline-
880 based extrapolation of past median values using the procedure specified in p.1496 of J&T2011 (p.62 of
881 T&J2012). It appears that this procedure has actually been used since then to generate the near-real time PC
882 index values presented at the AARI web portal (http://pcindex.org) and the ISGI web site
883 (http://isgi.unistra.fr). These PC index values have been shown to display excessive excursions with respect
884 to the corresponding post-event (final) index series (Stauning, 2018a).

885 In spite of specific statements to the opposite, neither Fig. 6 nor Fig. 7 of J&T2011 (Figs. 4.15 and 4.16 of
886 T&J2012) present near-real time values of the solar wind sector terms. They both, most likely, present values
887 derived by post-event methods as inferred from Figs. A4-A9 of this appendix.

888 Actually, none of the 8 figures in J&T2011 (T&J2012) displays near-real time values or derived results. Figs.
889 1, 6, 7, and 8 display values derived by post-event calculations based on daily medians from 7 days centred
890 on the day of interest. Figs. 2, 3, and 4 display values smoothed over 7 days, while the remaining Fig. 5
891 displays averages over 4 months.

892

893

Appendix A2 (for the review process only).

Appendix A2 presents further examples of erroneous archival PCS data like the one displayed in Fig. 12 of the manuscript. Examples with quiet conditions have been selected for display as the unjustified PCS excursions are then easy to detect. PCN/PCS examples have been downloaded from the graphical output of the otherwise excellent AARI web site http://pcindex.org and from the ISGI portal http://isgi.unistra.fr on 27 January 2020. The corresponding PCN and PCS index series derived by using the DMI post-event calculation methods are displayed in the bottom diagrams.

A2-1. PCN/PCS 26-30 June 2011

a. AARI archival web:

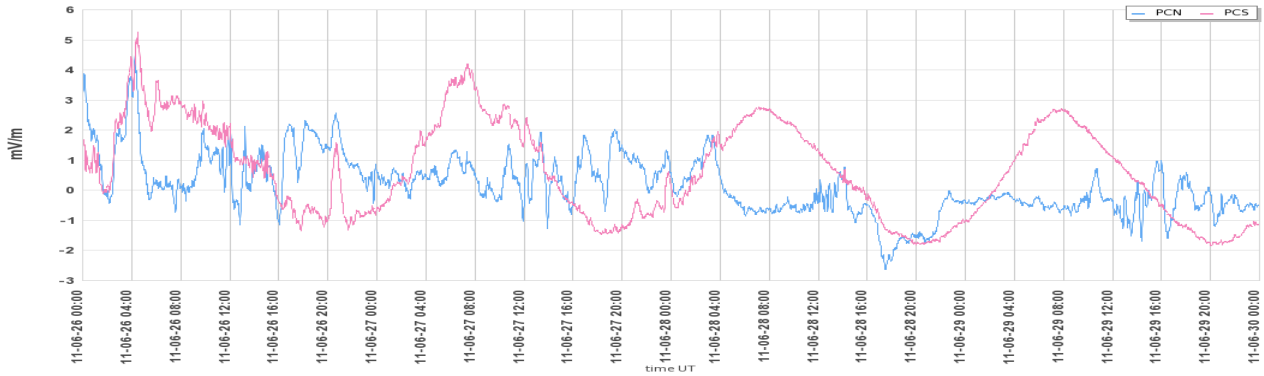

b. ISGI archival web:

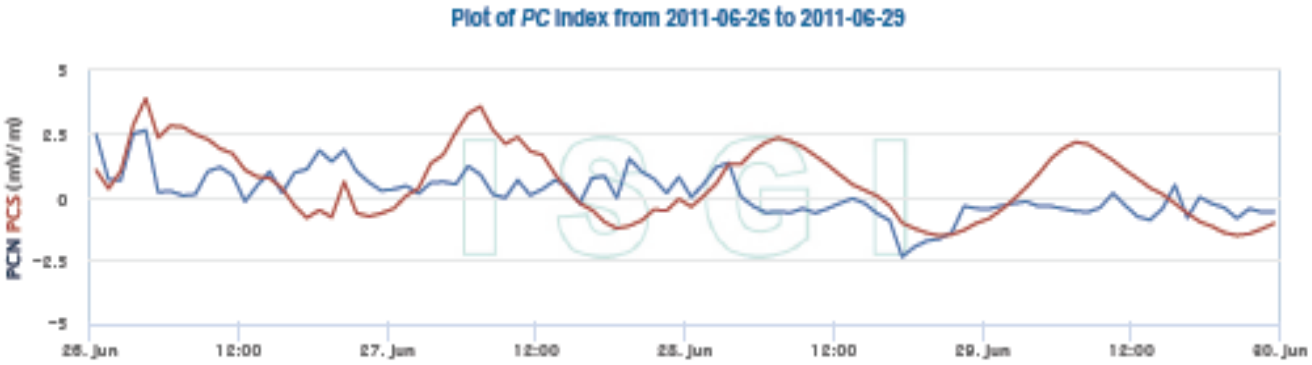

c. DMI post-event calculations:

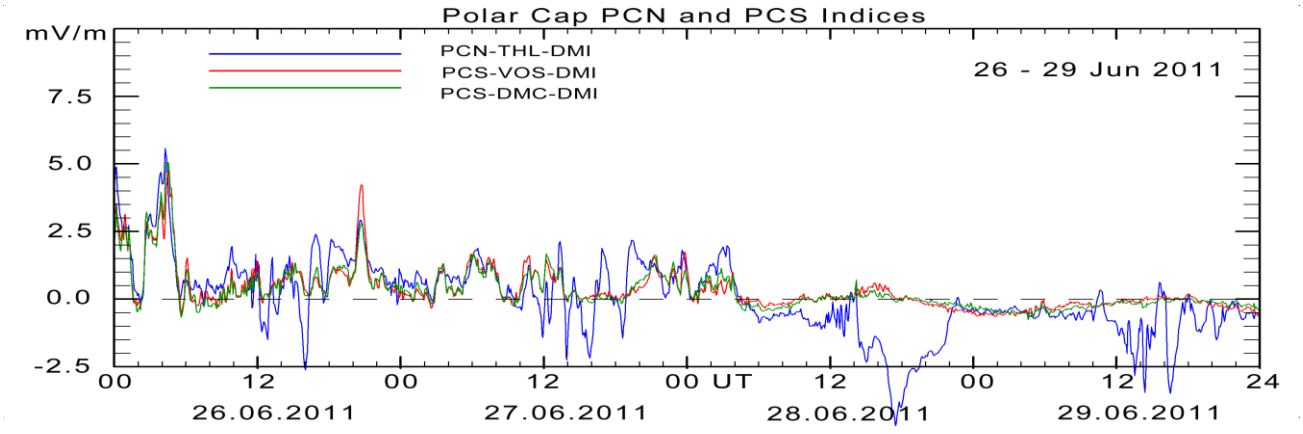

A2-2. PCN/PCS 23-26 September 2011

a. AARI archival web:

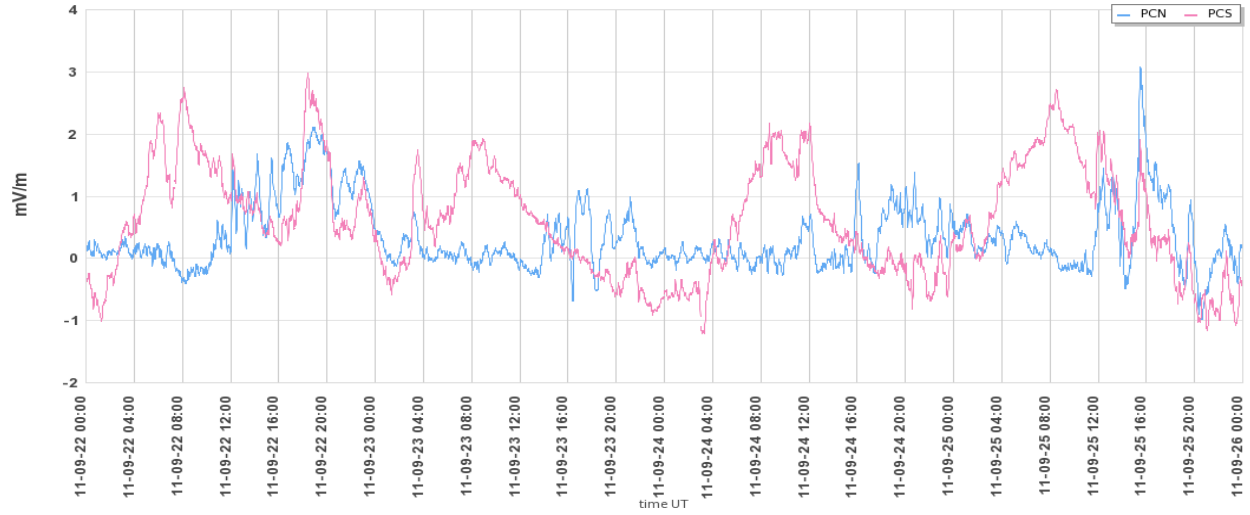

b. ISGI archival web:

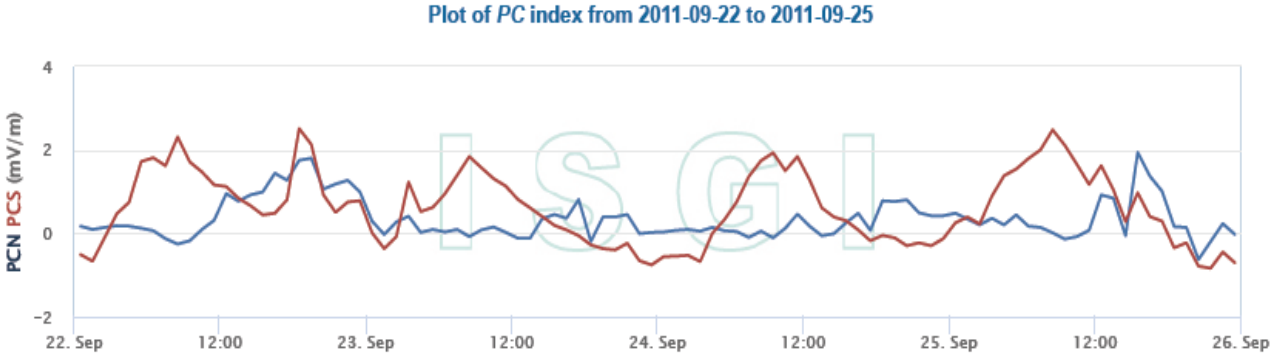

c. DMI post-event calculations:

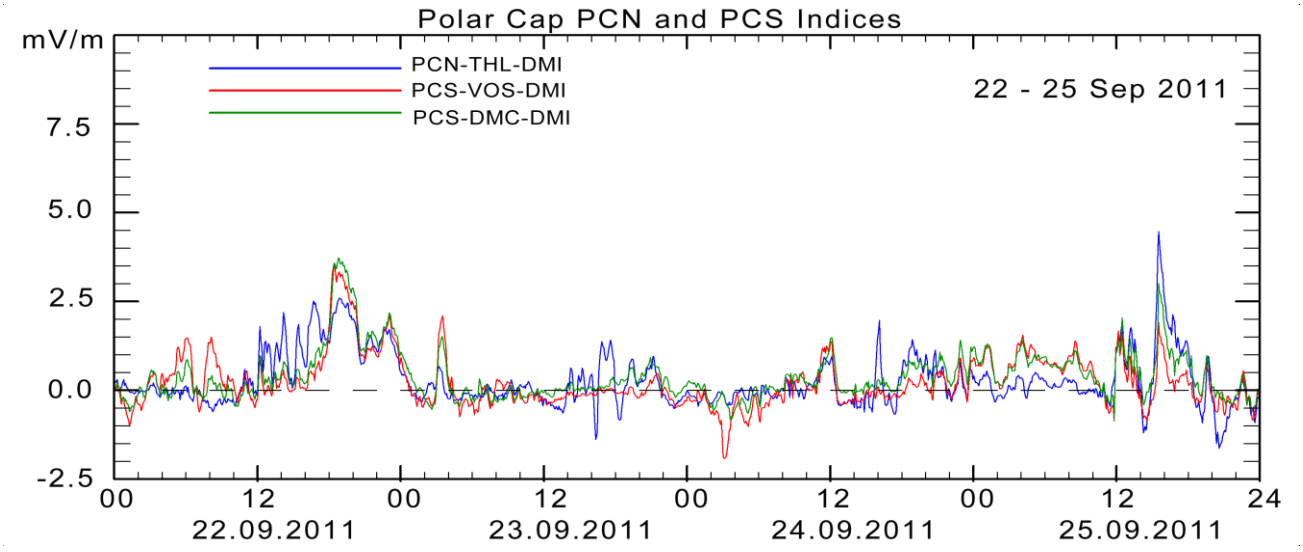

A2-3. PCN/PCS 17-21 November 2011

a. AARI archival web:

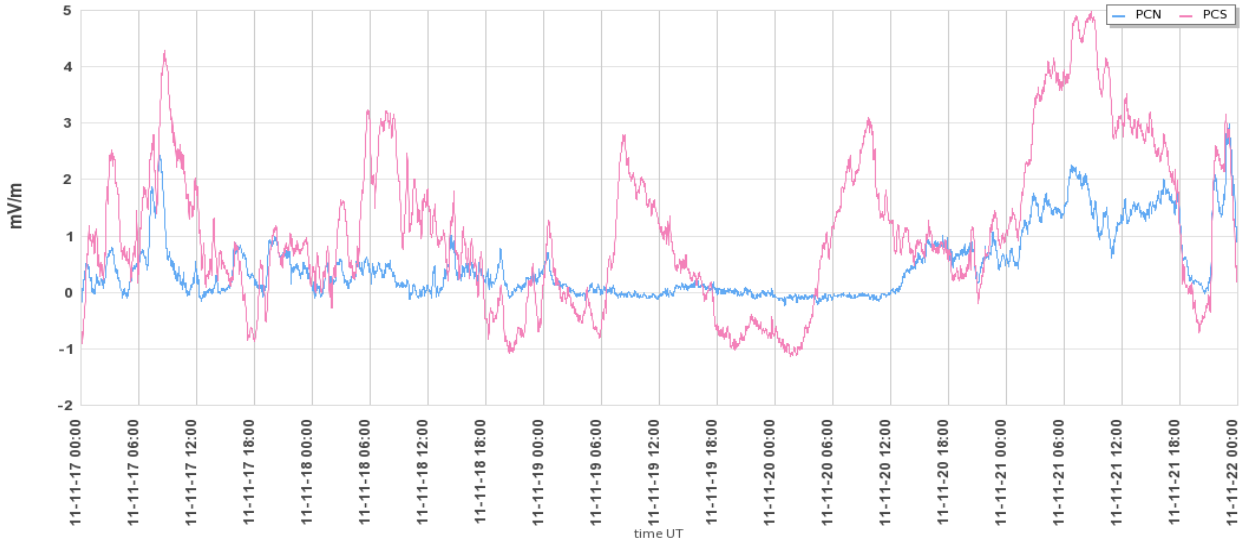

b. ISGI archival web:

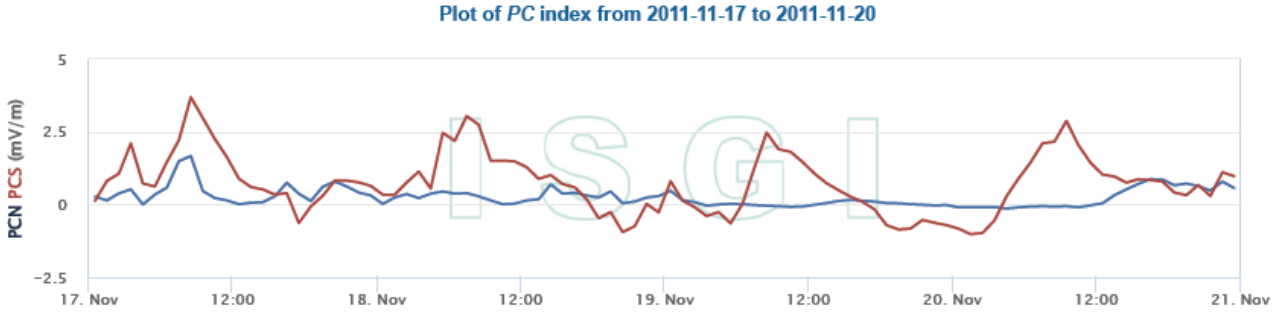

c. DMI post-event calculations:

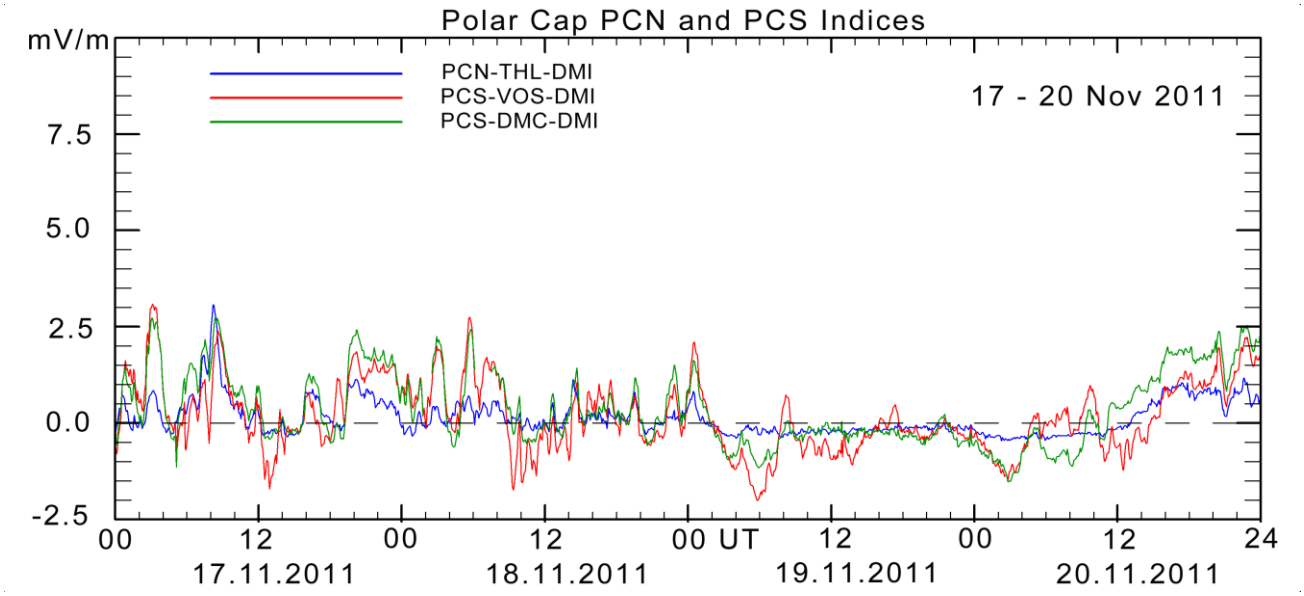

A2-4. PCN/PCS 15-18 December 2011 (also in Fig. 12 of manuscript)

a. AARI archival web:

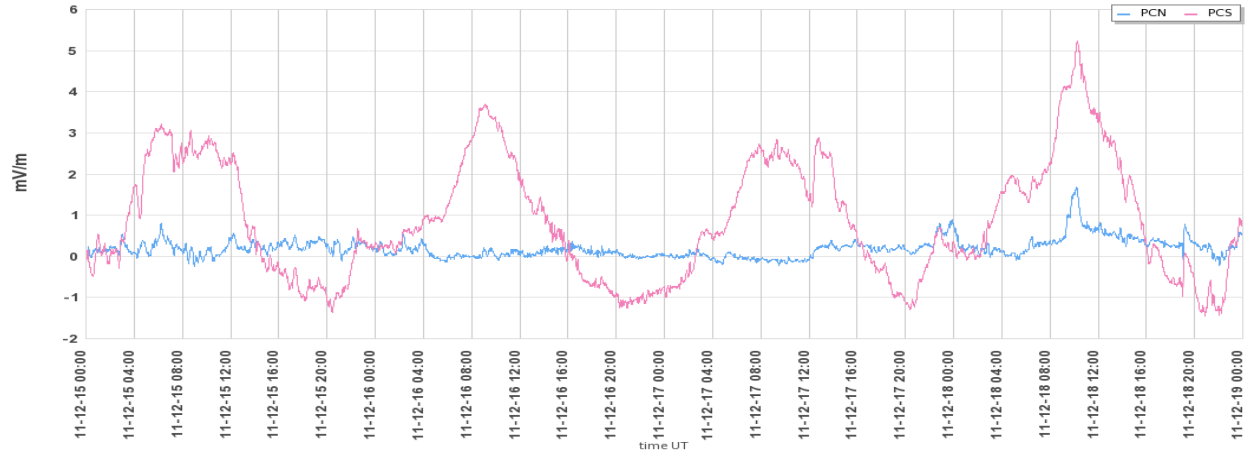

b. ISGI archival web:

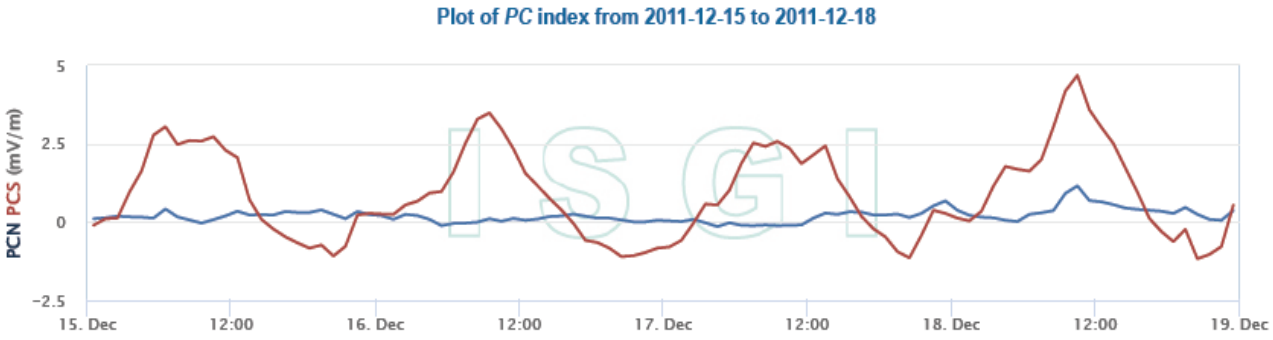

c. DMI post-event calculations

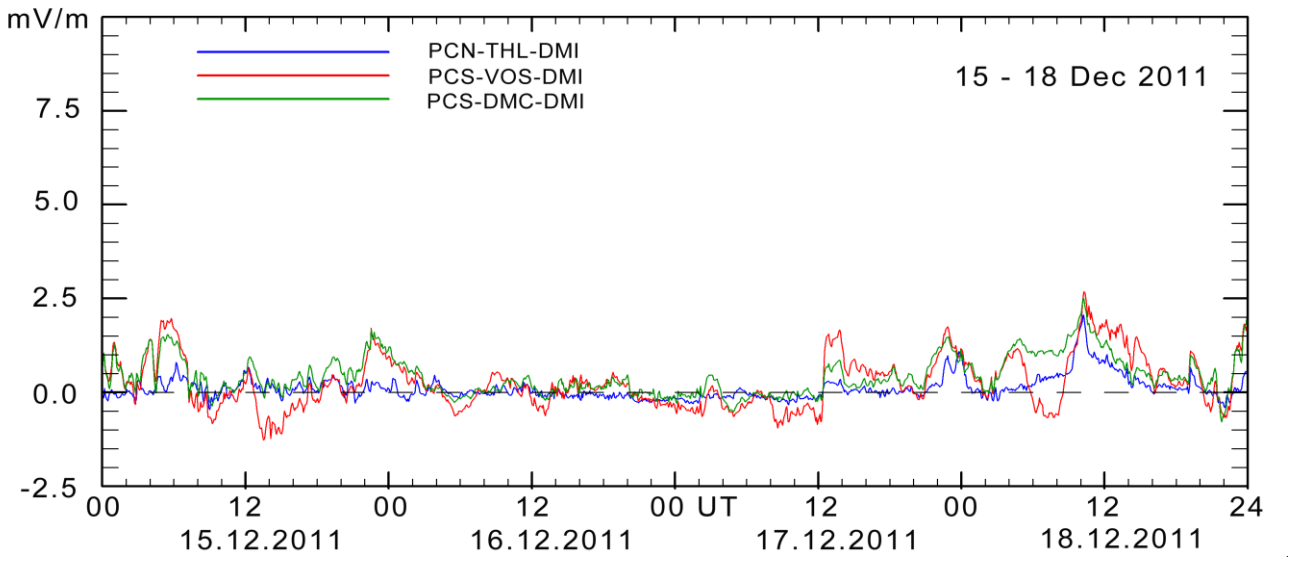

944 **A2-5. Summary.**

945 The PCS problem was detected in 2017 and notices of the problem was sent to the IAGA-approved
946 PC index suppliers, Arctic and Antarctic Research Institute (AARI) in St. Petersburg, Russia, and
947 DTU Space in Lyngby, Denmark during 2018. Notices have also been sent to the International
948 Service for Geomagnetic Indices (ISGI), and to IAGA representatives. The problem, furthermore,
949 was specified in the publication by Stauning (2018b).

950 The basic problem in the post-event (archival) PCS series displayed in Figs. A2-1a,b to A2-4,a,b of
951 appendix A2 is the occurrences of unjustified daily excursions ranging between appr. -1.5 and +4
952 mV/m. The real PCS variations appear to be superimposed on the erroneous daily excursions, Since
953 magnetic storm conditions are considered to apply at PC index levels exceeding 1.5 mV/m
954 (Troshichev et al., 2017), such excursions of up to 4 mV/m would indicate (or hide) strong
955 magnetic storms. The examples presented above are just a few among many corresponding cases in
956 the series of provisional PCS values. They have been selected because of their appearance during
957 quiet conditions, where the unfounded excursions are easy to detect. The magnetic data for these
958 examples have been obtained from INTERMAGNET data service (http://intermagnet.org), where
959 they are labeled as “final values”. It is difficult to assess the data handling problem at AARI since
960 there is no available description of the PCS derivation procedure.

961 Strictly speaking, the provisional PC index data should not be used in scientific works. However,
962 the index suppliers (AARI and ISGI) have not cautioned against the use of their PCS index series
963 and these indices have been used in several publications (e.g. Troshichev and Sormakov, 2015,
964 2017; Troshichev et al., 2014) without making notices of the potential problem.

965 With the DMI post-event data processing such excursions are absent as it appears from the PC
966 index plots at the bottom of each of the above pages. These plots present PCN values derived from
967 geomagnetic data from Qaanaaq (THL) in blue line. Furthermore, the plots indicate that the PCS
968 indices derived from Dome C data (green line) are close to the values derived from Vostok data (red
969 line). Thus, using both sources for deriving comparable PCS indices might enhance the reliability of
970 using the indices for Space Weather applications as well as in general geophysical studies
971 (Stauning, 2018b).

972

973